

# An improved and innovative formulation for calculating amplified elastic story drift induced by RBS connections in steel moment frames



Nader Fanaie<sup>\*</sup>, Shervin Safaei Faegh, Fatemeh Partovi

Department of Civil Engineering, K. N. Toosi University of Technology, Tehran, Iran

## ARTICLE INFO

### Article history:

Received 6 January 2019

Received in revised form 6 June 2019

Accepted 7 June 2019

Available online xxx

### Keywords:

Reduced beam section

Steel moment frames

Amplification factor of elastic story drift

Response surface method

Virtual work

## ABSTRACT

In recent years, the prequalified rigid connections of radius-cut reduced beam section (RBS) have been widely used in the design and construction of steel moment frames. Despite extensive investigations performed on the seismic performance of RBS connections, there is little research into the impact of these connections upon the elastic story drift in steel moment frames. In the current study, a precise formulation (partially based on a previous research) has been developed so as to evaluate the amount of stiffness variation or amplified elastic drift introduced by radius-cut RBS connections in a story of steel moment frames. Herein, by defining a novel and accurate method along with the method of virtual work, the amplified elastic drift of a 2-dimensional one-story single-span moment frame due to utilizing radius-cut RBS connections is calculated. The reliability and accuracy of the presented approach are validated using finite element modeling of the moment frame. Sensitivity analyses are also conducted upon the RBS connection parameters to derive the most effective parameters on the amount of elastic drift in steel moment frames. Then, by employing a statistical approach called response surface method (RSM) and combining findings of this study with some premises considered in a previous research, rigorous amplification factor of elastic drift formulas based on utilizing each of IPE and HEA beams in a story (from the first to the last one) with RBS connections are developed. Ultimately, two simple, linear, and functional amplification factor of elastic story drift formulas for each set of IPE and HEA story beams with RBS connections are proposed for designers. The scope of these formulas will be expanded to plate girders as well.

© 2019 Elsevier Ltd. All rights reserved.

## 1. Introduction

Typically, rigid connections play a remarkable role in providing stiffness, ductility, and stability in steel moment frames. Field observations and reports presented after 1994 Northridge earthquake in California, illustrated the widespread damage in the directly welded beam-to-column rigid connections of steel structures owing to the brittle and sudden fracture of full penetration groove welds, especially at the lower flange of the beams. Lack of sufficient ductility in the beam near the connection region is reckoned as one of the most important reasons for fracture in these connections [1]. Among the proposed solutions, providing the required ductility and controlled yielding zone through the weakening of beam flanges at specified sections has attracted various researchers' attention [2–7]. The mentioned solution is intended to transfer the location of energy dissipation and yielding (structural fuse) from the column face into the beam span as well as preventing the destruction of full penetration groove welds in directly welded beam-to-column connections of steel moment frames.

By performing numerous experimental tests on sub-assembly models of the steel frame with constant flange cut-out RBS connections and concrete slab system in some specimens, Plumier et al. [2] investigated the ductility, strength, and number of inelastic cycles in the specimens subjected to cyclic loading. As reported, RBS connections are capable of concentrating plastic deformations as well as providing adequate ductility in beam span, away from column face. Iwankiw et al. [3] and Chen et al. [4] examined the stiffness, strength, and ductility of taper-cut (according to the slope of seismic moment diagram of the beam) RBS connections subjected to cyclic loading, and suggested this kind of connection to achieve a uniform and relatively large yielding at specific locations of girders. In order to mitigate adverse consequences of stress concentration at reentrant corners of RBS connections, Engelhardt et al. [5] recommended employing radius-cut RBS as a viable and cost-effective solution in comparison with other alternatives. Furthermore, Popov et al. [6] conducted a number of laboratory experiments and nonlinear finite element modeling to investigate the fracture mode, state of triaxial loading and harmful effects of utilizing backing bar in directly welded beam-to-column connections (pre-Northridge earthquake connections). Based on these studies, they recommended the use of radius-cut RBS connections as an efficient way to improve the performance of steel connections in moment frames.

<sup>\*</sup> Corresponding author at: K.N. Toosi University of Technology, Civil Engineering Department, No. 1346, Vali-Asr Street, P.O. Box. 15875-4416, 19697 Tehran, Iran.  
E-mail address: fanaie@kntu.ac.ir (N. Fanaie).

The various shapes of cutting implemented in RBS connections are illustrated in Fig. 1.

Montuori [7] focused on the setting up a group of design rules that establish a correlation among the RBS locations, the geometry of cut-out sections and vertical gravity loads with the aim of limiting the formation of plastic hinges in the expected sections, i.e. in the dog-bones and/or in the intermediate beam sections. The philosophy of this research is based on the protection of beam-to-column connections in any conditions. Castaldo et al. [8] found it beneficial to employ dog-bone cut-outs in an innovative dissipative column. The objective of their research was to obtain further stiffness, strength, and damping that could come from the forming lever mechanism by the dissipated reduced section columns installed inside or outside of steel structures.

Generally, in first-order analyses, either manually or by structural design software, it is a routine and easy way to obtain the elastic displacement of a structure, and then multiplying a coefficient to this displacement can take other factors such as nonlinear effects into account. Although extensive studies have been carried out by different researchers to detect the seismic performance of radius-cut RBS connections [5–7,9], there are limited studies to develop an accurate analytical method calculating the influence of these connections on the elastic stiffness and drift of a story in steel moment frames. Chambers et al. [10] derived the stiffness matrix of a beam with radius-cut RBS connections using virtual work method [11] in which merely flexural and axial deformations were considered, and used the obtained stiffness matrix in the finite element modeling of six-story moment frames with two and three spans. By taking limited ranges of  $0.25d \leq a \leq 0.5d$  and  $0.75d \leq b \leq d$  (where  $d$  denotes beam depth and parameters  $a$ , and  $b$  are shown in Fig. 1) with maximum flange reduction of 40% into account, they finally came up with a maximum 10.6% increase in the elastic story drift of steel moment frames. Through using a simplified analytical approach based on equal flange elongation over the RBS region along with the portal method [12], Lee and Chung [13] converted the radius cut RBS to a straight cut RBS with equivalent length of  $b_{eq}$ , and then presented a set of equations to compute amplified elastic drift of a typical story in steel moment frames with RBS connections. AISC 358–16 Prequalified Connections [14] has suggested that instead of using analyses containing details of the RBS connections which may not always be available, the amount of effective elastic drift can be approximately estimated via multiplying the elastic drift of intended story based on gross beam section by 1.1 for flange reduction up to 50%. The linear interpolation may be implemented for lower amounts of beam flange reduction. Consequently, given proposed ranges for the RBS connection parameters in this design code, the amount of the elastic story drift amplification starts at 4% and ultimately reaches 10%.

It appears that introducing a precise formulation to determine the amount elastic drift amplification or the percentage of stiffness variations because of using RBS connections in a common story of steel moment frames, can pave the way for more accurate design and control of steel moment frames, on the other hand, it leads to an in-depth understanding of RBS connections' elastic behavior. This study aims to provide an exact formulation for determining the amplified elastic drift in a typical story of steel moment frames induced by radius-cut RBS connections. Consequently, in light of this approach two simple, linear and precise formulas are also proposed to estimate the amplification factor of elastic story drift regarding the type of beam used in the story. To this end, first, an exact approach alongside virtual work method [11] is presented for calculating elastic drift of a one-story single-span steel moment frame with radius-cut RBS connections which is capable of being (and should be) solved by existing mathematical software. Then, by performing sensitivity

analyses, some parameters of the RBS connection having by far the greatest impact on the elastic drift response of steel moment frames are specified. With respect to these parameters, proposed approach in Section 2 and premises taken in a previous authentic research, precise amplification factor of elastic story drift formulas for each IPE and HEA profiles which are extensively used as beam members in steel moment frames, are derived through a statistical approach known as response surface method. Finally, two distinct linear formulas covering all profiles of IPE and HEA (used as the beam with radius-cut RBS connections in a story) are presented to compute the percentage of elastic drift amplification or stiffness reduction at the story. Also, some conditions will be offered to extend the applicability of these formulas even to built-up beam sections. These formulas can be readily implemented by engineers, either in a manual or software design process.

## 2. A new procedure for calculation of elastic drift in a two-dimensional one-story single-span steel moment frame with radius-cut RBS connections

In this section, first, using the analytical method of virtual work [11] in a 2-dimensional one-story single-span steel moment frame with directly welded beam-to-column rigid connections subjected to the lateral force of  $P$  (Fig. 2(a)), the exact amount of elastic drift is determined. Referring to Fig. 2(b), the desired moment frame can be turned into a half-frame with the help of structural analysis rules relating to symmetric structures with anti-symmetric loadings.

By using the compatibility equation for equality of rotation on two sides of the node B, the internal moment of  $M$  is calculated as follows:

$$\theta_{B_L} = \theta_{B_R} \rightarrow \frac{P}{2} \frac{L_c^2}{2EI_c} - \frac{ML_c}{EI_c} = \frac{M}{3EI_b} \rightarrow \frac{M}{6E} \left( \frac{6L_c}{I_c} + \frac{L_b}{I_b} \right) = \frac{PL_c^2}{4EI_c} \rightarrow M = \frac{1.5PL_c^2}{\frac{6L_c}{I_c} + \frac{L_b}{I_b}} \quad (1)$$

where  $P$  is the lateral shear force applied to the moment frame,  $L_c$  and  $L_b$  are the column length and beam length (distances between centerlines), respectively,  $E$  (200,000 MPa) is the elastic modulus of used steels,  $I_c$  and  $I_b$  are the moment of inertia of the column and beam about the bending axis (strong axis), respectively, and  $M$  is the internal bending moment in node B in the case of directly welded beam-to-column rigid connections. According to the bending moment obtained from Eq. (1), the amount of elastic drift in the intended steel moment frame with directly welded beam-to-column rigid connections which is merely caused by flexural deformations, is calculated by Eq. (2):

$$\Delta_{Bending} = \frac{PL_c^3}{6EI_c} - \frac{ML_c^2}{2EI_c} \quad (2)$$

As the analysis of the moment frame's forces is demonstrated in Fig. 3, amounts of the elastic drift due to shear and axial deformations of the frame members regarding the selection of the same profiles for the beam and columns, are calculated by Eqs. (3) and (4), respectively.

$$\Delta_{Shear} = \int \frac{V(x)v(x)}{GA_s} dx = \sum \frac{VvL}{GA_s} = 2 \times \frac{P}{2} \cdot \frac{1}{2} \cdot L_c + \frac{2M}{L_b} \cdot \frac{2M}{PL_b} \cdot L_b = \frac{PL_c}{2} + \frac{4M^2}{PL_b} \quad (3)$$

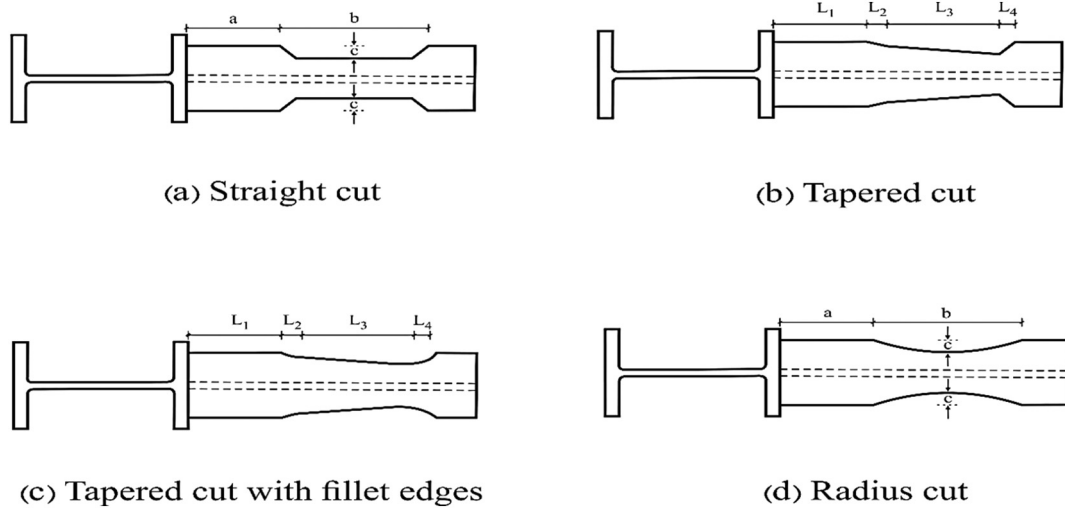


Fig. 1. Different configurations of RBS connection.

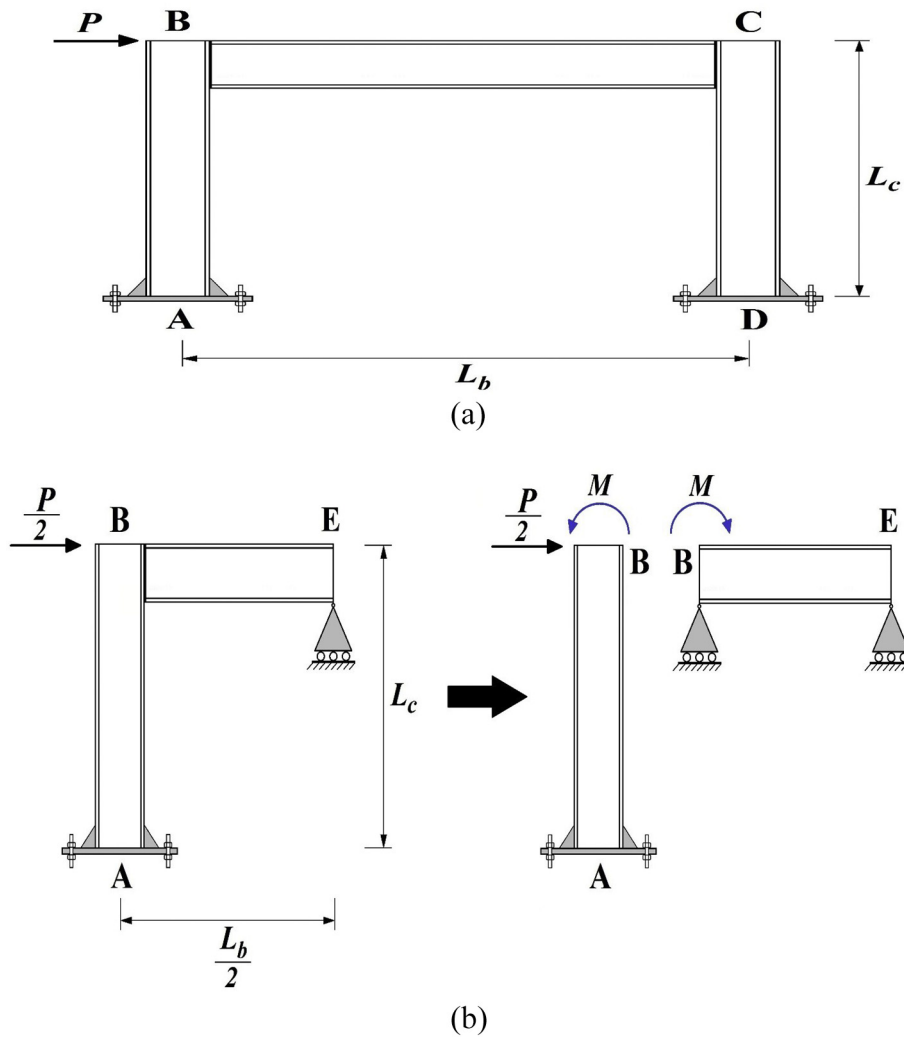


Fig. 2. Analysis of the steel moment frame through changing it into two half-frames: (a) Desired steel moment frame with directly welded rigid connections and (b) The half-frame resulting from splitting the steel moment frame.

$$\Delta_{Axial} = \int \frac{N(x)n(x)}{AE} dx = \sum \frac{NnL}{AE} = 2 \times \frac{2M}{L_b} \cdot \frac{2M}{PL_b} \cdot L_c = \frac{8M^2 L_c}{PL_b^2 A_c E} \quad (4)$$

where  $G = \frac{E}{2(1+\nu)}$  is the shear modulus of elasticity,  $\nu = 0.3$  is the Poisson's ratio,  $A_c$  is the cross-sectional area of the columns, and  $A_s$  is the effective shear cross-sectional area of the beam or columns that for I sections is equal to the cross-section area of web ( $h_w \cdot t_w$ ). Finally, by summation of Eq. (2), Eq. (3) and Eq. (4), the total amount of elastic drift for the steel moment frame with directly welded rigid connections under the lateral force of  $P$ , is calculated as follows:

$$\Delta_{total} = \Delta_{Bending} + \Delta_{Shear} + \Delta_{Axial} = \frac{PI_c^3}{6EI_c} - \frac{MI_c^2}{2EI_c} + \frac{P^2 L_c L_b + 8M^2}{2PL_b GA_s} + \frac{8M^2 L_c}{PL_b^2 A_c E} \quad (5)$$

Considering radius-cut RBS connections for the intended steel moment frame with the geometrical characteristics depicted in Fig. 4(a), the rotation value in the right side of node B will be achieved greater than the value calculated in Eq. (1). Thus, following reproducing a half-frame from the moment frame with RBS connections (Fig. 4(b)), using the virtual work method [11] via applying a unit moment to node B (Fig. 4(c)) and the equality of internal work with external work done in the half-beam, the amount of rotation in the right side of node B with regard to employment of RBS connections,  $\theta_{B_R}'$ , is expressed in Eq. (6).

$$1 \times \theta_{B_R}' = \int_0^{\frac{L_b}{2}} \frac{M(x)m(x)}{EI(x)} dx = \int_0^{\frac{L_b}{2}} \frac{2M'x}{L_b} \cdot \frac{2x}{L_b} dx = \frac{4M'}{EL_b^2} \int_0^{\frac{L_b}{2}} x^2 dx \quad (6)$$

where  $I(x)$  is the moment of inertia of the half-beam varying along the half-beam length,  $M'$  is the internal bending moment in node B considering RBS connections for the frame. Given the geometry and location of the RBS connection in the half-beam span, the integral of Eq. (6) is re-written as follows:

$$\theta_{B_R}' = \theta_1' + \theta_2' + \theta_3' \quad (7)$$

$$\theta_1' = \frac{4M'}{EL_b^2 I_b} \int_0^{\frac{L_b}{2}-a-b} x^2 dx \quad (8)$$

$$\theta_2' = \frac{4M'}{EL_b^2} \int_{\frac{L_b}{2}-a-b}^{\frac{L_b}{2}-a} \frac{x^2}{I(x)} dx \quad (9)$$

$$\theta_3' = \frac{4M'}{EL_b^2 I_b} \int_{\frac{L_b}{2}-a}^{\frac{L_b}{2}} x^2 dx \quad (10)$$

where:

$$I_b = \frac{1}{12} [b_f(h_w + 2t_f)^3 - (b_f - t_w)h_w^3] \quad (11)$$

$$I(x) = \frac{1}{12} [b(x)(h_w + 2t_f)^3 - (b(x) - t_w)h_w^3] \quad (12)$$

$$b(x) = b_f + 2R - 2c - 2\sqrt{R^2 - \left(x - \left(\frac{L_b}{2} - a - \frac{b}{2}\right)\right)^2} \quad (13)$$

The parameters of the RBS connection ( $a$ ,  $b$ ,  $c$ , and  $R$ ) and the geometrical characteristics of the I beam section ( $b_f$ ,  $h_w$ ,  $t_f$ , and  $t_w$ ) are illustrated in Fig. 4(a). Incorporating Eqs. (11)–(13) into Eqs. (7)–(10)

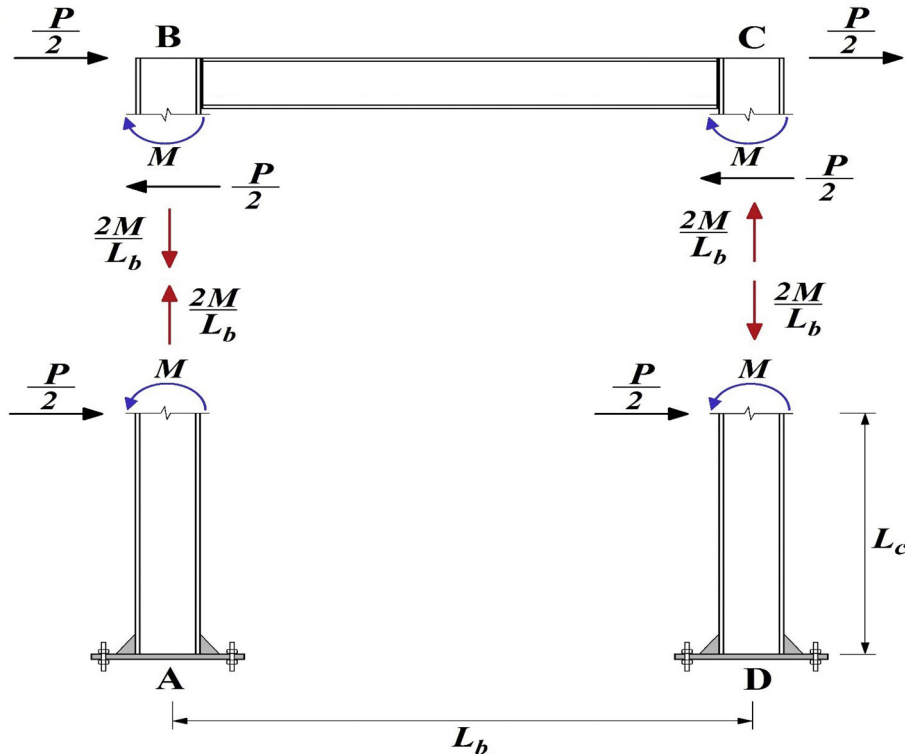


Fig. 3. Distribution and analysis of the steel moment frame's internal forces under the lateral force of  $P$ .

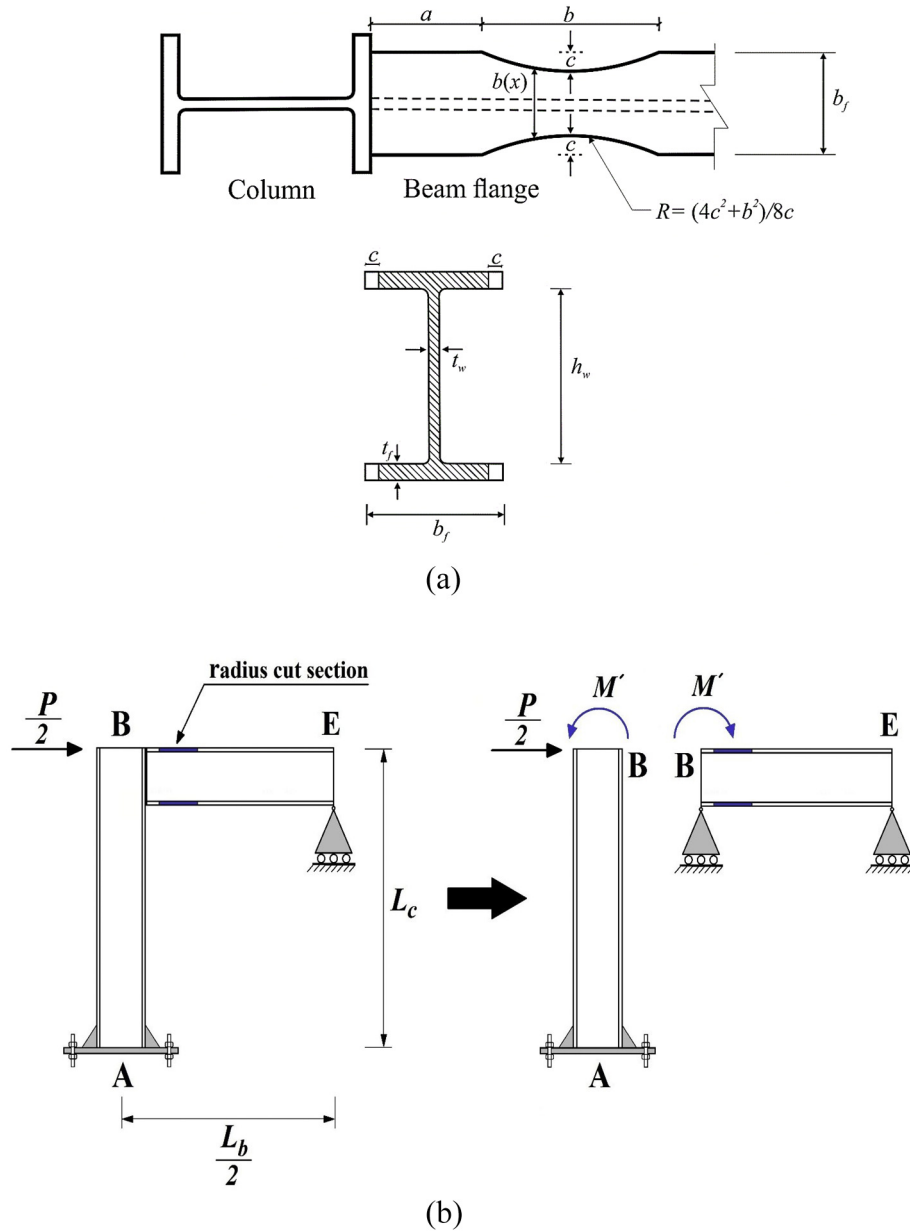


Fig. 4. Geometrical characteristics of radius-cut RBS connections and analysis of the half-beam with the RBS connection using the virtual work method: (a) Details of radius-cut RBS connections, (b) The half-frame resulting from splitting the steel moment frame with RBS connections and (c) Moment diagrams of the half-beam with the RBS connection used in the virtual work method.

regenerates the constituent terms of Eq. (7) as follows:

$$\theta'_1 = \frac{4M'}{12 [b_f(h_w + 2t_f)^3 - (b_f - t_w)h_w^3]} \times \frac{\left(\frac{L_b}{2} - a - b\right)^3}{3} \quad (14)$$

$$\theta'_2 = \frac{4M'}{EL_b^2} \left[ \int_{\frac{L_b}{2} - a - b}^{\frac{L_b}{2} - a} \frac{x^2 dx}{12 \left[ \left( b_f + 2R - 2c - 2\sqrt{R^2 - \left( x - \left( \frac{L_b}{2} - a - \frac{b}{2} \right) \right)^2} \right) (h_w + 2t_f)^3 - \left( b_f + 2R - 2c - 2\sqrt{R^2 - \left( x - \left( \frac{L_b}{2} - a - \frac{b}{2} \right) \right)^2} - t_w \right) h_w^3 \right]} \right] \quad (15)$$

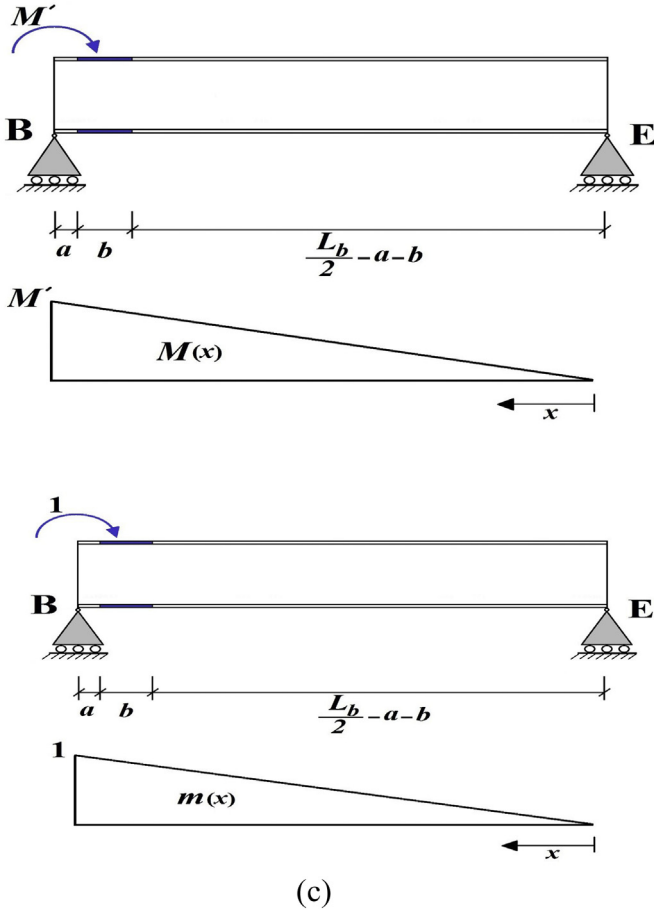


Fig. 4 (continued).

$$\theta'_3 = \frac{4M'}{12 [b_f(h_w + 2t_f)^3 - (b_f - t_w)h_w^3]} \times \frac{\left(\frac{L_b}{2}\right)^3 - \left(\frac{L_b}{2} - a\right)^3}{3} EL_b^2 \quad (16)$$

Despite the employment of a theoretically routine and simple approach to obtain the value of  $\theta'_2$ , it was found that the integral in Eq. (15) has no numerical solution even by assigning numbers to all parameters (except for the independent variable of  $x$ ) in powerful mathematical software such as Maple [15] or Matlab [16]. This problem is circumvented through adopting the following method to achieve a numerical response from Eq. (9). As observed in Fig. 5(a), the amount of  $c(\alpha)$  along the radius cut can be calculated as:

$$\begin{aligned} c(\alpha) &= R \cdot \cos\alpha - (R - c) = \left(\frac{b^2 + 4c^2}{8c}\right) \cdot \cos\alpha - \left(\frac{b^2 + 4c^2}{8c} - c\right) \\ &= \left(\frac{b^2 + 4c^2}{8c}\right) \cdot \cos\alpha - \left(\frac{b^2 - 4c^2}{8c}\right) \end{aligned} \quad (17)$$

Consequently, the variation of the beam flange width over the RBS cut,  $b(x)$ , is redefined by Eq. (17) and Fig. 5(a):

$$\begin{aligned} b(x) &= b_f - 2c(x) \rightarrow b(\alpha) = b_f - 2c(\alpha) \\ &= b_f - \left(\frac{b^2 + 4c^2}{4c}\right) \cdot \cos\alpha + \left(\frac{b^2 - 4c^2}{4c}\right) \end{aligned} \quad (18)$$

According to Fig. 5(b),  $\cos\alpha$  can be taken as a function of  $x$ , as follows:

$$h(x) = x - \left(\frac{L_b}{2} - a - \frac{b}{2}\right) = x + a + \frac{b}{2} - \frac{L_b}{2} \quad \left(\frac{L_b}{2} - a \leq x \leq \frac{L_b}{2} - a - b\right) \quad (19)$$

$$\begin{aligned} \tan\alpha &= \frac{h(x)}{R - c} = \frac{x + a + \frac{b}{2} - \frac{L_b}{2}}{\frac{b^2 + 4c^2}{8c} - c} = \frac{x + a + \frac{b}{2} - \frac{L_b}{2}}{\frac{b^2 - 4c^2}{8c}} \\ &= \frac{8c \cdot \left(x + a + \frac{b}{2} - \frac{L_b}{2}\right)}{(b + 2c)(b - 2c)} \end{aligned} \quad (20)$$

$$\begin{aligned} \cos\alpha &= \frac{1}{\sqrt{1 + \tan^2\alpha}} = \frac{1}{\sqrt{1 + \frac{64 \cdot c^2 \cdot \left(x + a + \frac{b}{2} - \frac{L_b}{2}\right)^2}{(b + 2c)^2 (b - 2c)^2}}} \\ &= \frac{1}{\sqrt{\frac{(b + 2c)^2 (b - 2c)^2 + 64 \cdot c^2 \cdot \left(x + a + \frac{b}{2} - \frac{L_b}{2}\right)^2}{(b + 2c)^2 (b - 2c)^2}}} \\ &= \frac{(b + 2c)(b - 2c)}{\sqrt{(b + 2c)^2 (b - 2c)^2 + 64 \cdot c^2 \cdot \left(x + a + \frac{b}{2} - \frac{L_b}{2}\right)^2}} \end{aligned} \quad (21)$$

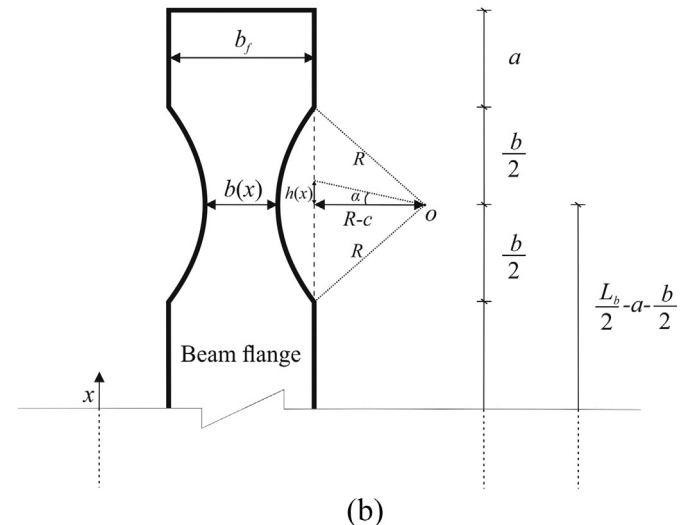
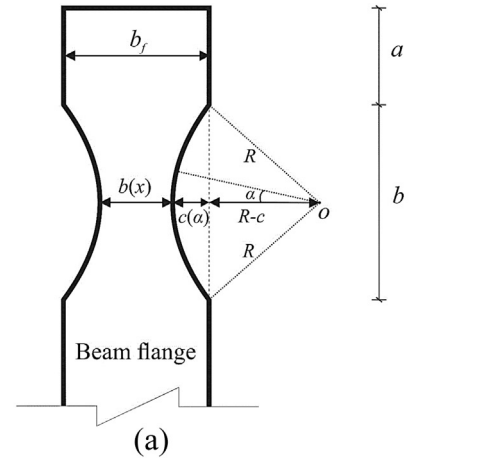


Fig. 5. Defining specific geometric notations for a typical radius-cut on the beam flange.

Combining Eqs. (9), (12), (18), and (21) results in the following equation for calculation of  $\theta_2'$ :

$$\theta_2' = \frac{4M'}{EI_c^2} \int_{\frac{b}{2}-a}^{\frac{b}{2}-a} x^2 dx = \frac{4M'}{EI_c^2} \int_{\frac{b}{2}-a}^{\frac{b}{2}-a} I(x) \frac{x^2 dx}{12} \left[ \left( b_f - \left( \frac{b^2 + 4c^2}{4c} \right) \cdot \frac{(b+2c)(b-2c)}{\sqrt{(b+2c)^2(b-2c)^2 + 64c^2 \left( x + a + \frac{b}{2} - \frac{b_f}{2} \right)^2}} + \left( \frac{b^2 - 4c^2}{4c} \right) \right) (h_w + 2t_f)^3 - \left( b_f - \left( \frac{b^2 + 4c^2}{4c} \right) \cdot \frac{(b+2c)(b-2c)}{\sqrt{(b+2c)^2(b-2c)^2 + 64c^2 \left( x + a + \frac{b}{2} - \frac{b_f}{2} \right)^2}} + \left( \frac{b^2 - 4c^2}{4c} \right) - t_w \right) h_w^3 \right] \quad (22)$$

By replacing Eqs. (14), (16) and (22) in Eq. (7), and assigning numbers to all parameters (except for the moment of  $M'$ ), the exact value of  $\theta_{B_r}'$  using Maple mathematical software [15] can be assessed as a function of  $M'$ . Maple software [15] is a powerful mathematical software for solving mathematical problems as well as engineering calculations and has the outstanding capability of solving integrals. Following determination of  $M'$  by applying the compatibility equation as shown in Eq. (23), the elastic drift of the steel moment frame with RBS connections considering only flexural deformations,  $\Delta_{Bending}'$ , is expressed as follows:

$$\theta_{B_r}' = \theta_{B_r} \rightarrow \frac{P}{2EI_c} L_c^2 - \frac{M'L_c}{EI_c} = \theta_{B_r}' \rightarrow M' = f(P, L_c, L_b, I_c, b_f, t_f, h_w, t_w, a, b, c, E) \quad (23)$$

$$\Delta_{Bending}' = \frac{PL_c^3}{6EI_c} - \frac{M'L_c^2}{2EI_c} \quad (24)$$

The shear and axial deformations affected by RBS connections in the intended steel moment frame are achieved by means of replacing the bending moment of  $M'$  instead of  $M$  in Eq. (3), Eq. (4), respectively. Therefore, the summation of these two equations with Eq. (24) provides the following formula to determine the total elastic drift of the desired steel moment frame with RBS connections under the lateral load of  $P$ , with respect to having the same sections for the beam and columns:

$$\Delta_{total}' = \Delta_{Bending}' + \Delta_{Shear}' + \Delta_{Axial}' = \frac{PL_c^3}{6EI_c} - \frac{M'L_c^2}{2EI_c} + \frac{P^2 L_c L_b + 8M'^2}{2PL_b G A_s} + \frac{8M'^2 L_c}{PL_b^2 A_c E} \quad (25)$$

Ultimately, the amplification factor of elastic drift due to the use of RBS connections in the one-story single-span steel moment frame is calculated as follows:

$$Amp_{f-1} = \frac{\Delta_{total}'}{\Delta_{total}} = \frac{\frac{PL_c^3}{6EI_c} - \frac{M'L_c^2}{2EI_c} + \frac{P^2 L_c L_b + 8M'^2}{2PL_b G A_s} + \frac{8M'^2 L_c}{PL_b^2 A_c E}}{\frac{PL_c^3}{6EI_c} - \frac{ML_c^2}{2EI_c} + \frac{P^2 L_c L_b + 8M^2}{2PL_b G A_s} + \frac{8M^2 L_c}{PL_b^2 A_c E}} \quad (26)$$

It should be noted due to the existence of the direct relationship between the moments of  $M$  and  $M'$  with the force of  $P$ , this force has no influence on the amplification factor of elastic drift and can be omitted from Eq. (26).

### 3. Finite element modeling and verification

The finite element analyses by ABAQUS software [17] were conducted to evaluate the reliability and accuracy of Eq. (26). To this end, two one-story single-span steel moment frames under the lateral force of  $P$  which is equal to 25 tons, in cases of with and without RBS connections were modeled (shown in Fig. 6(a) and (b)). The story height and span length (centerline to centerline distances) of the moment frames are equal to 350 cm and 600 cm, respectively. The same I-shaped built-up profiles with the geometric parameters presented in Table 1 were used as the beams and columns. To prevent any instabilities in the frames members in the forms of local and global buckling caused by the lateral force of 25 tons, the built-up profile conforms to AISC 360 and AISC 341 seismic design procedure [18,19]. Moreover, due to the examination of inter-story drift only in the elastic stage of the steel moment frames, yielding stresses of the members were

taken extremely large amounts to ensure their elastic behavior in the finite element modeling. The values of the RBS connections parameters are listed in Table 1 and selected using AISC 358–16 prequalified connections [14] proposed ranges, as follows:

$$0.5b_{bf} \leq a \leq 0.75b_{bf} \quad (27)$$

$$0.65d \leq b \leq 0.85d \quad (28)$$

$$0.1b_{bf} \leq c \leq 0.25b_{bf} \quad (29)$$

where  $d = h_w + 2t_f$  is the height of the beam. Eurocode 8 [20] has also provided some limits for the RBS connection parameters, but these limits originate from AISC 358–16 prequalified connections [14] limited ranges, thus there is no significant difference between these two codes.

The steel moment frames in two cases of with and without RBS connections were modeled using 4-node shell elements (S4R). This element has 6 degrees of freedom per node and is capable of predicting the behavior of slender members precisely, especially I-shaped steel profiles, in the light of using the reduced integration in time-saving analyses. Assuming that the desired moment frames are two-dimensional, out of plane displacement of the frames was completely restrained in the finite element modeling. The base plates were also completely fixed by modeling clamped supports. In the finite element analyses, geometrical nonlinearities effects have been ignored because of the theoretical premises adopted in calculating the elastic drift of the frames. Utilizing structured quad elements and partitioning techniques led to generating meshes that are completely regular with a suitable aspect ratio in all members of the frames and helped to achieve desirable responses (Fig. 6(c)). Force control static general analyses alongside Maple software [15] were utilized to draw a comparison between the amplification factor of elastic drift resulting from the finite element modeling of the frames with that resulting from Eq. (26), in Table (2).

As reported in Table 2, the percent error between the elastic drifts derived from the developed equations in this study and the numerical modeling results is 1.17% in the case of using RBS connections and 1.53% in the case of without using the RBS connections. These very small amounts of error are negligible and indicate the correctness as well as the adequate accuracy of the developed theoretical formulas for predicting the exact value of elastic drift or stiffness changes in a one-story single-span steel moment frame in states of with or without RBS connections. It should be pointed out that the source of this negligible story drift discrepancy between the finite element simulation responses and those of the presented formulas for the one-story single-span modeled frame is mainly due to the panel zone deformations which will be thoroughly addressed in Section 5 as well as common and inevitable errors normally occurred in the finite element software. In addition, the aforementioned comparison shows justification of utilizing the variable moment of inertia along the RBS region ( $I(x)$ ) for calculating the amplification factor of elastic drift in a typical story (every desired story) of steel moment frames with radius-cut RBS connections in subsequent sections.

### 4. Sensitivity analysis of RBS's parameters

Selected values for the geometric parameters of RBS connections ( $a$ ,  $b$ , and  $c$ ) have influence on the elastic drift and lateral stiffness of story,

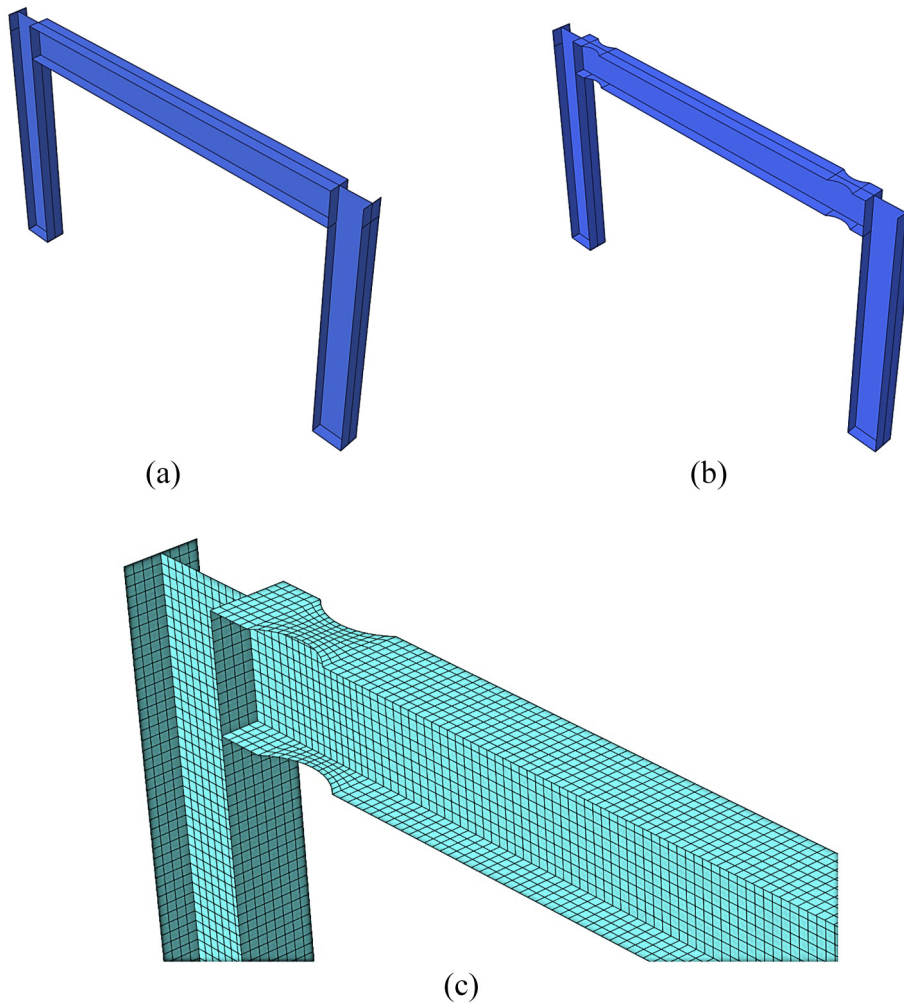


**Fig. 6.** Modeled steel moment frames in the finite element software: (a) with direct beam-to-column rigid connections (without RBS connections), (b) with RBS connections and (c) Typical FEM mesh on a model.

but the impact magnitude of each parameter is different from the other ones. With the purpose of creating accurate and optimal formulas for determining the amplification factor of elastic drift or percentage of stiffness reduction in a story of steel moment frames with RBS connections, first, it is attempted to specify the minimum number of RBS connection parameters having the greatest impacts on the elastic drift for utilizing in the RSM method. In this section, by conducting sensitivity analyses upon the *a*, *b*, and *c* parameters using Maple software [15] and Eq. (25), the effect of each parameter on the elastic drift of the one-story single-span steel moment frame with RBS connections (used in the previous section, Fig. 6(a)), subjected to the lateral force of  $P = 25$  tons is discussed. For this purpose, two beams of IPE profiles (300, 600) and two beams of HEA profiles (500, 1000) are selected to explore the effects of variation in each of the RBS connection parameters on the elastic drift of the desired moment frame regarding the described ranges in Eqs. (27)–(29). During sensitivity analyses, all other parameters except the intended parameter are kept constant in the mean value of their range. Note that profiles of the beam and columns are

considered the same in the frame. The results of the sensitivity analyses in Figs. 7–10 show that the increase in the RBS connection parameters values in all cases changes the elastic drift of the desired steel moment frame in an approximately linear procedure. By comparing the slopes in the linear graphs of elastic lateral drift depicted in Figs. 7–10, it is concluded that the parameter *c* has the greatest effect on the elastic drift of steel moment frames, and then the parameter *b*, but the parameter *a* effect is negligible. In addition, by increasing the height to width ratio of the beam profiles, the effect of the parameter *c* on the elastic drift progressively increases compared with the effect of the parameter *b*. Thus in the remainder of this study, only two parameters *b* and *c* will be addressed in the formulas that determine the amplification factor of elastic drift in a story of steel moment frames with RBS connections.

**5. Derivation of formulas in order to calculate the amplification factor of elastic drift in a story based on using HEA or IPE beams with RBS connections**

The objective of this section is to derive simple and functional formulas for computing the amplification factor of elastic drift induced by RBS connections in a typical story of steel moment frames. To achieve this, two widely used groups of IPE and HEA beams, which are widespread in the steel structure industry in various countries, are selected to be used in a subassembly proposed by Lee and Chung [13] but with the same beam and column, as displayed in Fig. 11. With the help of the portal method [12] (formation of plastic hinges in the mid-span of

**Table 1**  
Geometrical characteristics of the beams, columns and RBS connections.

Built-up profiles' geometry parameters				RBS's parameters		
$h_w$ (cm)	$b_f$ (cm)	$t_f$ (cm)	$t_w$ (cm)	<i>a</i> (cm)	<i>b</i> (cm)	<i>c</i> (cm)
42	32	3	1.5	20	40	7.5

**Table 2**  
Comparison of numerical results with developed formulas results.

Analysis type	Flexural deformations (mm)	Shear deformations (mm)	Axial deformations (mm)	Elastic drift (mm)	
Theoretical (with RBS connections)	3.617	1.053	0.016	4.686	1.025
Theoretical (without RBS connections)	3.491	1.062	0.017	4.57	1.022
ABAQUS (with RBS connections)	–	–	–	4.741	–
ABAQUS (without RBS connections)	–	–	–	4.64	–

beams and columns) accompanied by panel zone distortion theory [21], they formulated the elastic story drift of steel moment frames consisting of simultaneous contribution of the column ( $\delta_c$ ), the panel zone ( $\delta_{pz}$ ), and the beam ( $\delta_b$ ) to the drift:

$$\delta_{total} = \delta_c + \delta_{pz} + \delta_b \tag{30}$$

$$\delta_c = \frac{V_c(H_c - d_b)^3}{12EI_c} \tag{31}$$

$$\delta_{pz} = \frac{V_c H_c (H_c - d_b)}{Gd_b d_c t_{pz}} \tag{32}$$

$$\delta_b = \int_0^{\frac{L_b}{2}} \frac{V_c H_c \left(\frac{L_b}{2} - x\right) / (L_b + d_c)}{EI(x)} dx \times \left( 1 - \left( \frac{2 \int_0^{\frac{L_b}{2}} \frac{V_c H_c \left(\frac{L_b}{2} - x\right) x / (L_b + d_c)}{EI(x)} dx}{(L_b + d_c) \times \int_0^{\frac{L_b}{2}} \frac{V_c H_c \left(\frac{L_b}{2} - x\right) / (L_b + d_c)}{EI(x)} dx} + \frac{d_c}{(L_b + d_c)} \right) \right) \times H_c \tag{33}$$

Where  $V_c$  and  $V_b$  are the column shear force and the beam shear force, respectively,  $L_b$  is the beam span length and  $H_c$  is the story height,  $d_c$  and  $d_b$  are the height of the column and beam, respectively,  $I_c$  is the moment of inertia of the column, and  $t_{pz}$  is equal to the panel zone thickness. Outside of the RBS connection region,  $I(x)$  is equal to the moment of inertia of the beam ( $I_b$ ), otherwise inspired by the presented method for calculating the variable moment of inertia along the RBS region in Section 2,  $I(x)$  is calculated as follows:

$$I'(x) = \frac{1}{12} \left[ \left( b_f - \left( \frac{b^2 + 4c^2}{4c} \right) \cdot \frac{(b+2c)(b-2c)}{\sqrt{(b+2c)^2(b-2c)^2 + 64.c^2.(x-a-\frac{b}{2})^2}} + \left( \frac{b^2 - 4c^2}{4c} \right) \right) (h_w + 2t_f)^3 - \left( b_f - \left( \frac{b^2 + 4c^2}{4c} \right) \cdot \frac{(b+2c)(b-2c)}{\sqrt{(b+2c)^2(b-2c)^2 + 64.c^2.(x-a-\frac{b}{2})^2}} + \left( \frac{b^2 - 4c^2}{4c} \right) - t_w \right) . h_w^3 \right] \tag{34}$$

Finally, by considering Eqs. (30–34), the amplification factor of elastic drift in a story of steel moment frames having RBS connections is computed by Eq. (35).

$$Amp = \frac{\delta_b + \frac{(H_c - d_b)^3}{12EI_c} + \frac{H_c(H_c - d_b)}{Gd_b d_c t_{pz}}}{\int_0^{\frac{L_b}{2}} \frac{H_c \left(\frac{L_b}{2} - x\right) / (L_b + d_c)}{EI_b} dx \times \left( 1 - \left( \frac{2 \int_0^{\frac{L_b}{2}} \frac{H_c \left(\frac{L_b}{2} - x\right) x / (L_b + d_c)}{EI_b} dx}{(L_b + d_c) \times \int_0^{\frac{L_b}{2}} \frac{H_c \left(\frac{L_b}{2} - x\right) / (L_b + d_c)}{EI_b} dx} + \frac{d_c}{(L_b + d_c)} \right) \right) \times H_c + \frac{(H_c - d_b)^3}{12EI_c} + \frac{H_c(H_c - d_b)}{Gd_b d_c t_{pz}}} \tag{35}$$

where:

$$\delta'_b = \int_0^a \frac{H_c \left(\frac{L_b}{2} - x\right) / (L_b + d_c)}{EI_b} dx \times \left( 1 - \left( \frac{2 \int_0^{\frac{L_b}{2}} \frac{H_c \left(\frac{L_b}{2} - x\right) x / (L_b + d_c)}{EI_b} dx}{(L_b + d_c) \times \int_0^{\frac{L_b}{2}} \frac{H_c \left(\frac{L_b}{2} - x\right) / (L_b + d_c)}{EI_b} dx} + \frac{d_c}{(L_b + d_c)} \right) \right) \times H_c + \int_a^{a+b} \frac{H_c \left(\frac{L_b}{2} - x\right) / (L_b + d_c)}{EI'(x)} dx \times \left( 1 - \left( \frac{2 \int_0^{\frac{L_b}{2}} \frac{H_c \left(\frac{L_b}{2} - x\right) x / (L_b + d_c)}{EI'(x)} dx}{(L_b + d_c) \times \int_0^{\frac{L_b}{2}} \frac{H_c \left(\frac{L_b}{2} - x\right) / (L_b + d_c)}{EI'(x)} dx} + \frac{d_c}{(L_b + d_c)} \right) \right) \times H_c + \int_{a+b}^{\frac{L_b}{2}} \frac{H_c \left(\frac{L_b}{2} - x\right) / (L_b + d_c)}{EI_b} dx \times \left( 1 - \left( \frac{2 \int_0^{\frac{L_b}{2}} \frac{H_c \left(\frac{L_b}{2} - x\right) x / (L_b + d_c)}{EI_b} dx}{(L_b + d_c) \times \int_0^{\frac{L_b}{2}} \frac{H_c \left(\frac{L_b}{2} - x\right) / (L_b + d_c)}{EI_b} dx} + \frac{d_c}{(L_b + d_c)} \right) \right) \times H_c \tag{36}$$

Note that the incorporation of Eqs. (12) and (13) into Eqs. (35) and (36) yields no numerical solution even by assigning numbers to all parameters in powerful mathematical software. Then, through the implementation of a statistical approach known as the response surface method, along with using Eq. (35), Maple [15] and Design Expert [22] software, distinct formulas are developed to calculate the amplification factor of elastic drift in a story of steel moment frames with RBS connections based on the type of used beam in this story. It should be noted

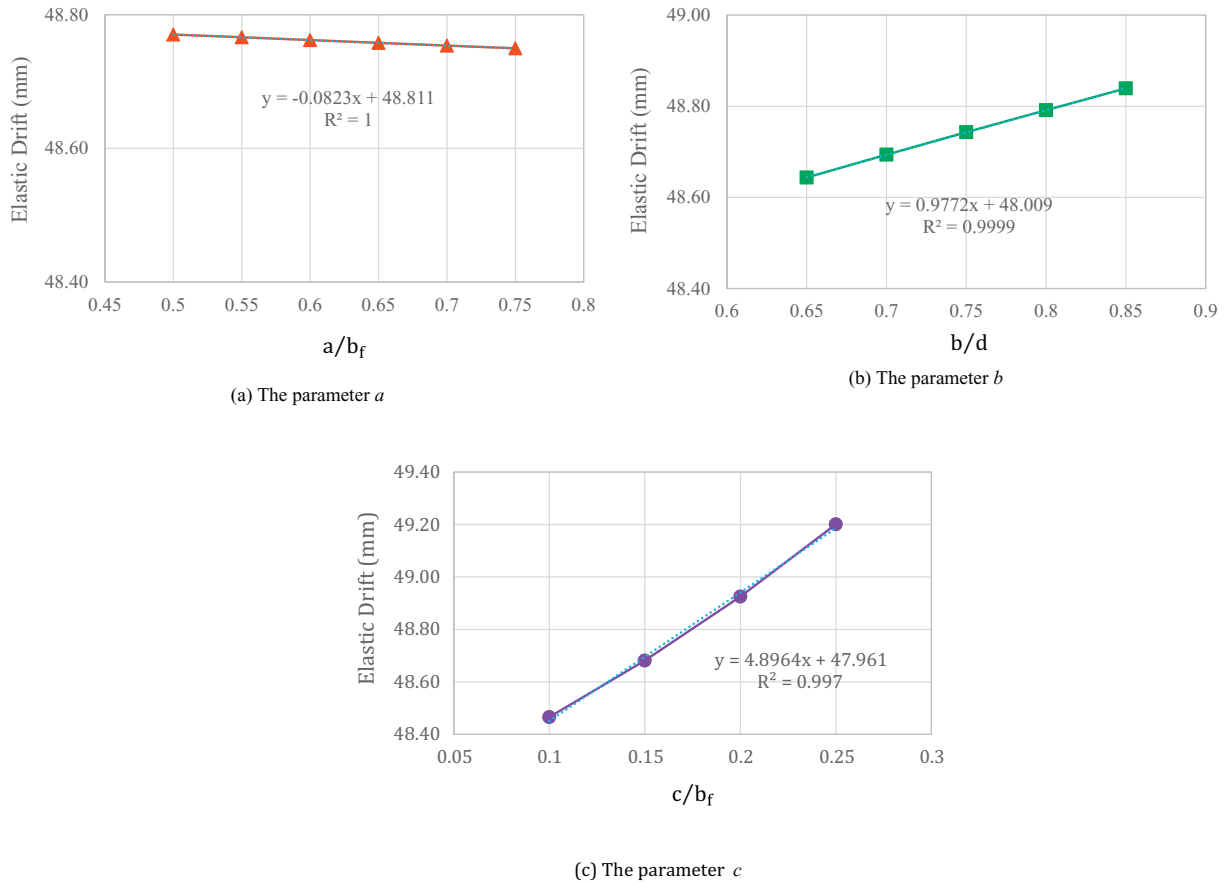


Fig. 7. Results of the sensitivity analyses on the RBS connection parameters when using IPE300 profile as the beam: (a) The parameter  $a$ , (b) The parameter  $b$  and (c) The parameter  $c$ .

that the story height and span length are equal to 350 cm and 600 cm, respectively, since being similar to a common story. The response surface method, as a reliable empirical modeling method, by designing a limited number of experiments can explore the relationship and interaction between explanatory variables and a response variable or, in general, describe overall system behavior in an optimal way. This method is generally applied to solve complex problems with numerous influential independent variables with the aim of achieving a reliable response regarding time and cost. Utilizing this method to estimate and identify the response surface requires designing an experiment. In this study designing the experiment is performed via the central composite design method (CCD), because this well-known method is appropriate to estimate second order polynomial responses. The Design Expert software [22] is one of the most versatile and rigorous software in designing the experiment for the RSM method, which has the ability to design an experiment in different ways, including the CCD method. Furthermore, this software has the capability of presenting an optimal formulation for a product or process. Given the sensitivity analyses performed in Section 4 and the limited ranges provided in Eqs. (27)–(29), the two parameters  $c$  and  $b$  which have the greatest effects on the elastic drift of steel moment frames, are used as explanatory variables and the amplification factor of elastic story drift in Eq. (35),  $Amp$ , is used as the response variable in the Design Expert software [22]. Subsequently, by designing 13 tests through the CCD method for each of HEA and IPE profiles as the story beam (collectively 546 tests), second-order formulas have been provided for calculating the amplification factor of elastic drift in a story of steel moment frames based on the used beam, in Tables 3 and 4. The unit of the parameters  $c$  and  $b$  in these formulas is centimeter. According to the statistical tests conducted in Design Expert software [22], all these second-order formulas have adjusted R-square

of about 0.99, minimum coefficient of variation and minimum standard deviation. In addition, the pure error and lack of fit values are approximately equal to zero in all presented formulas.

After obtaining the equations for calculating the amplification factor of elastic story drift based on the use of each of HEA and IPE beam profiles, the amplification factor of elastic story drift,  $Amp$ , versus the parameter  $c$  (in cm) which has the greatest effect on the story drift in steel moment frames, are plotted in different ratios of  $b/d$  for each of the mentioned beam profiles. The relationship between  $Amp$  and the parameter  $c$  in some selective samples of the IPE profiles, is depicted in Fig. 12. The corresponding graphs are constantly ascending with convex curvature in all IPE profiles.

In contrast to IPE profiles, the amplification factor of elastic story drift curves in HEA profiles have two different trends. The first trend consists of profiles up to the HEA300 having the height to flange width ratio of approximately one, and concave curves, as shown in Fig. 13. Also in these profiles, with the increase in the parameter  $c$  and approaching its value to the parameter  $R$  in the curves corresponded to the ratio of  $b/d = 0.65$ , the amount of the amplification factor of elastic story drift tends toward a constant number. The second trend includes profiles from the HEA320 to the HEA1000. As the height to flange width ratio of these profiles progressively increases from one, the amplification factor of elastic story drift curves gradually change from concave curvature to a linear state and then to the quadratic graphs with convex curvature.

After plotting all the amplification factor of elastic story drift curves as functions of the parameter  $c$  and the ratio of  $b/d$  for all IPE and HEA beam profiles, the curves with ratio of  $b/d = 0.85$  are chosen as dominant curves which have the position above the other curves in each of the mentioned beam profiles. These curves are put together in Fig. 14.

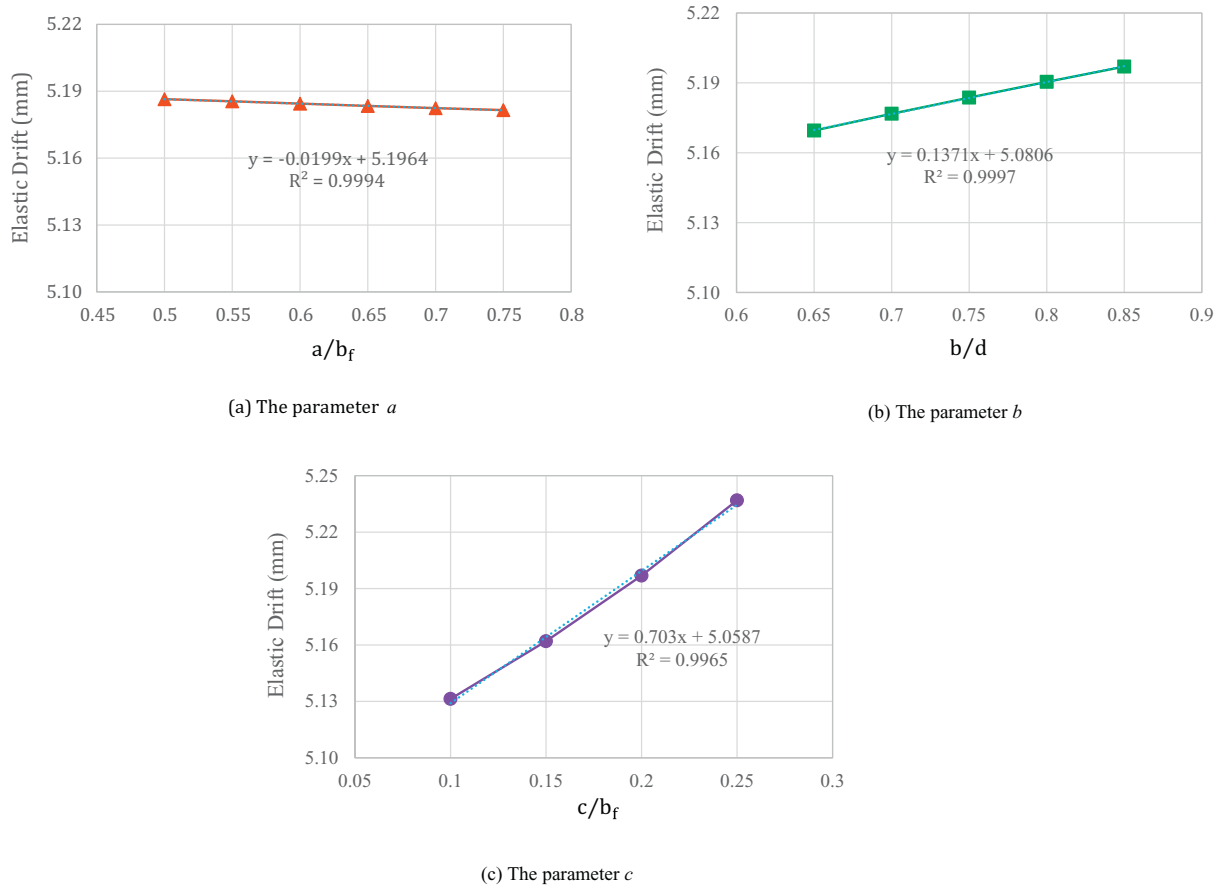


Fig. 8. Results of the sensitivity analyses on the RBS connection parameters when using IPE600 profile as the beam: (a) The parameter  $a$ , (b) The parameter  $b$  and (c) The parameter  $c$ .

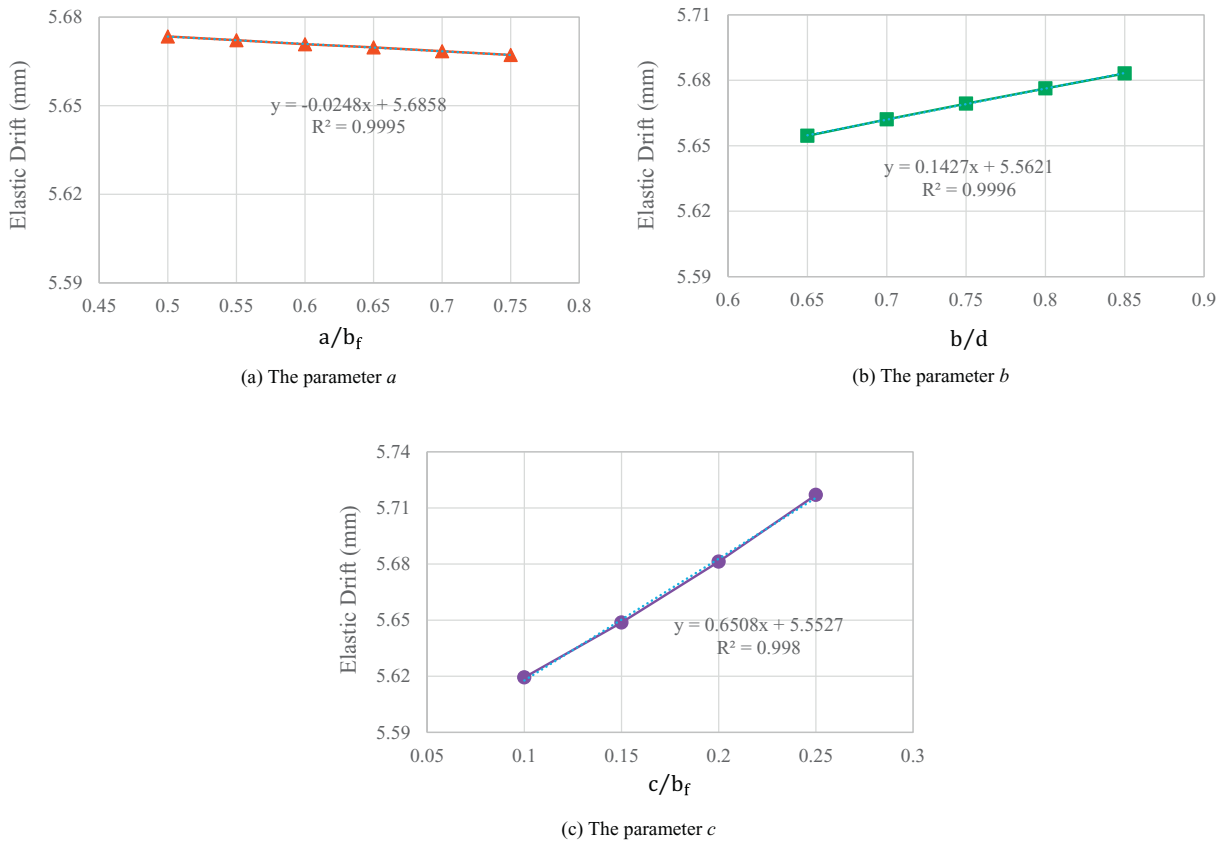


Fig. 9. Results of the sensitivity analyses on the RBS connection parameters when using HEA500 profile as the beam: (a) The parameter  $a$ , (b) The parameter  $b$  and (c) The parameter  $c$ .

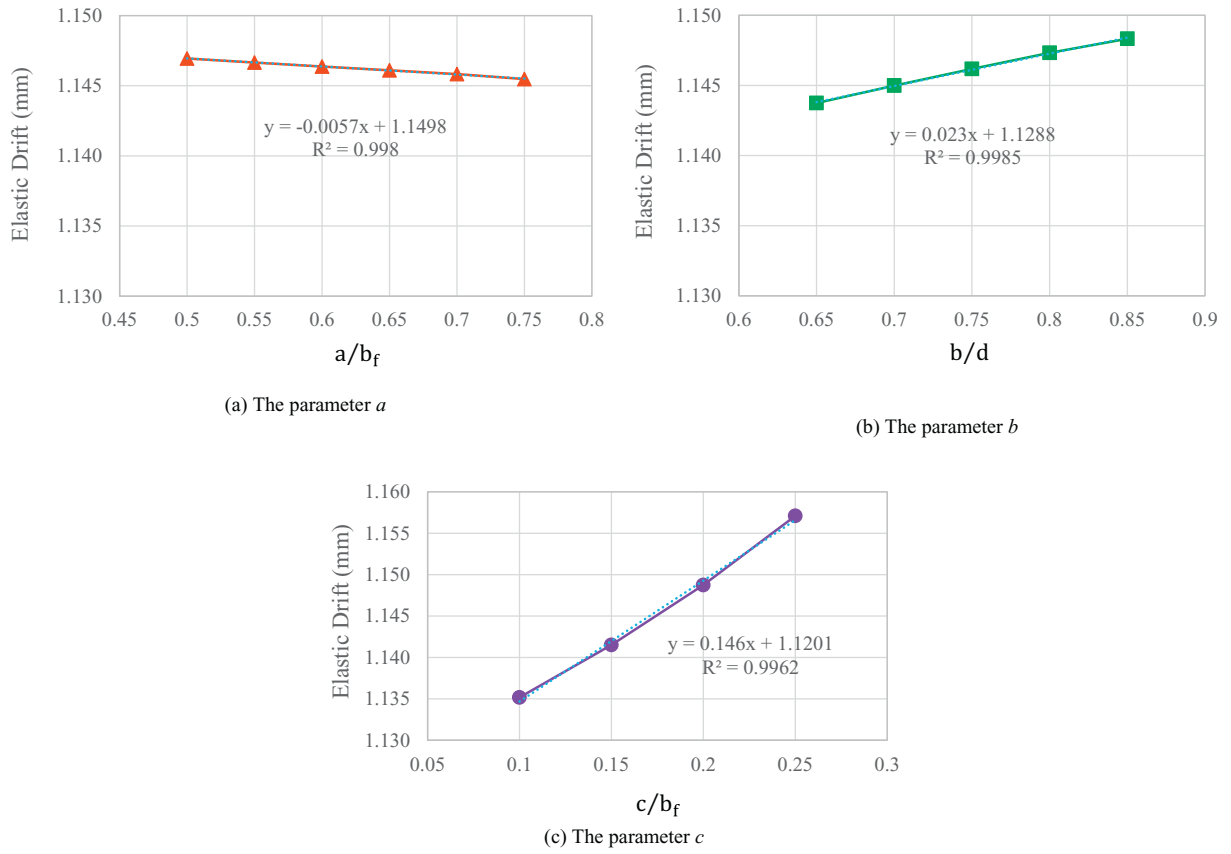


Fig. 10. Results of the sensitivity analyses on the RBS connection parameters when using HEA1000 profile as the beam: (a) The parameter  $a$ , (b) The parameter  $b$  and (c) The parameter  $c$ .

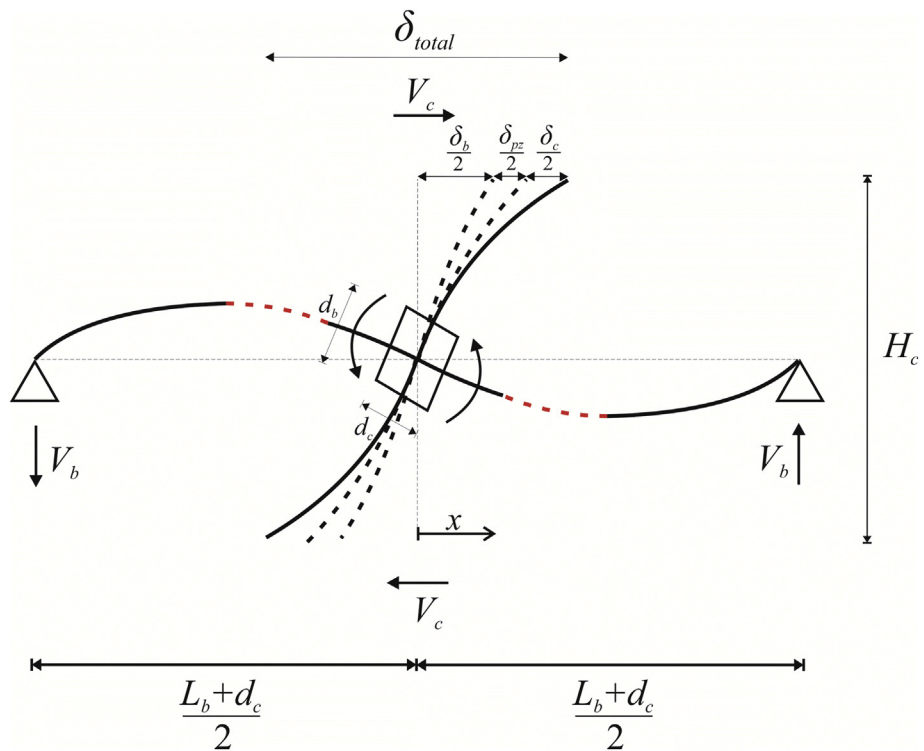


Fig. 11. Subassembly configuration for calculating inter-story drift induced by RBS connections by Lee and Chung [13]

**Table 3**  
Amplification factor of elastic story drift formulas for each IPE profile as the story beam with RBS connections.

Profile type	Amplification factor of elastic drift formula
IPE80	$Amp = 1.00352 - 2.56996 \times 10^{-4}b - 9.66230 \times 10^{-3}c + 2.97159 \times 10^{-3}bc - 2.31891 \times 10^{-5}b^2 + 3.20818 \times 10^{-3}c^2$
IPE100	$Amp = 1.00411 - 1.27737 \times 10^{-4}b - 9.64648 \times 10^{-3}c + 2.36728 \times 10^{-3}bc - 1.87123 \times 10^{-5}b^2 + 2.91458 \times 10^{-3}c^2$
IPE120	$Amp = 1.00460 - 1.41466 \times 10^{-4}b - 9.44517 \times 10^{-3}c + 1.92319 \times 10^{-3}bc - 1.54152 \times 10^{-5}b^2 + 2.59600 \times 10^{-3}c^2$
IPE140	$Amp = 1.00503 - 1.55015 \times 10^{-4}b - 9.20802 \times 10^{-3}c + 1.60293 \times 10^{-3}bc - 1.31677 \times 10^{-5}b^2 + 2.31139 \times 10^{-3}c^2$
IPE160	$Amp = 1.00546 - 7.28814 \times 10^{-5}b - 9.03088 \times 10^{-3}c + 1.37864 \times 10^{-3}bc - 1.19568 \times 10^{-5}b^2 + 2.07907 \times 10^{-3}c^2$
IPE180	$Amp = 1.00581 - 6.98999 \times 10^{-5}b - 8.78844 \times 10^{-3}c + 1.19154 \times 10^{-3}bc - 1.07346 \times 10^{-5}b^2 + 1.87172 \times 10^{-3}c^2$
IPE200	$Amp = 1.00616 + 2.34157 \times 10^{-5}b - 8.61559 \times 10^{-3}c + 1.05449 \times 10^{-3}bc - 1.01646 \times 10^{-5}b^2 + 1.70506 \times 10^{-3}c^2$
IPE220	$Amp = 1.00645 + 1.11123 \times 10^{-6}b - 8.30618 \times 10^{-3}c + 9.22531 \times 10^{-4}bc - 9.31956 \times 10^{-6}b^2 + 1.51048 \times 10^{-3}c^2$
IPE240	$Amp = 1.00677 + 8.33061 \times 10^{-5}b - 8.09677 \times 10^{-3}c + 8.25710 \times 10^{-4}bc - 9.03014 \times 10^{-6}b^2 + 1.36214 \times 10^{-3}c^2$
IPE270	$Amp = 1.00692 + 7.09948 \times 10^{-5}b - 7.50459 \times 10^{-3}c + 6.90097 \times 10^{-4}bc - 8.05643 \times 10^{-6}b^2 + 1.13229 \times 10^{-3}c^2$
IPE300	$Amp = 1.00699 + 6.35095 \times 10^{-5}b - 6.98094 \times 10^{-3}c + 5.86236 \times 10^{-4}bc - 7.28032 \times 10^{-6}b^2 + 9.56983 \times 10^{-4}c^2$
IPE330	$Amp = 1.00712 + 1.33396 \times 10^{-4}b - 6.86275 \times 10^{-3}c + 5.23972 \times 10^{-4}bc - 6.88237 \times 10^{-6}b^2 + 9.27391 \times 10^{-4}c^2$
IPE360	$Amp = 1.00716 + 1.19077 \times 10^{-4}b - 6.69672 \times 10^{-3}c + 4.66471 \times 10^{-4}bc - 6.27270 \times 10^{-6}b^2 + 8.90527 \times 10^{-4}c^2$
IPE400	$Amp = 1.00702 + 1.85161 \times 10^{-4}b - 6.50387 \times 10^{-3}c + 4.12714 \times 10^{-4}bc - 5.84738 \times 10^{-6}b^2 + 8.70305 \times 10^{-4}c^2$
IPE450	$Amp = 1.00664 + 1.89992 \times 10^{-4}b - 6.23131 \times 10^{-3}c + 3.57923 \times 10^{-4}bc - 5.17312 \times 10^{-6}b^2 + 8.53069 \times 10^{-4}c^2$
IPE500	$Amp = 1.00623 + 1.92171 \times 10^{-4}b - 5.97620 \times 10^{-3}c + 3.13493 \times 10^{-4}bc - 4.65243 \times 10^{-6}b^2 + 8.30389 \times 10^{-4}c^2$
IPE550	$Amp = 1.00573 + 2.40817 \times 10^{-4}b - 5.68632 \times 10^{-3}c + 2.78103 \times 10^{-4}bc - 4.38915 \times 10^{-6}b^2 + 7.98351 \times 10^{-4}c^2$
IPE600	$Amp = 1.00523 + 2.35596 \times 10^{-4}b - 5.43067 \times 10^{-3}c + 2.46805 \times 10^{-4}bc - 4.01941 \times 10^{-6}b^2 + 7.69027 \times 10^{-4}c^2$

By drawing envelopes of the two curves groups shown in Fig. 14 (a) and (b), two independent second-order formulas are developed to predict the amplification factor of elastic drift in a story having IPE or HEA beam and RBS connections. These prediction formulas are only in terms of the parameter  $c$  (in cm). In addition, so as to provide simple, practical and conservative equations which account uncertainties as well, two extra linear design formulas are proposed to estimate the amplification factor of elastic story drift based on using IPE or HEA beam. The prediction and design formulas for IPE profiles and HEA profiles are presented by Eqs. (37)–(40). Corresponding curves are depicted in Fig. 15 as well.

$$Amp_{IPE,Prediction} = 1 + 0.0143c - 0.0004c^2 \quad (37)$$

$$Amp_{IPE,Design} = 1 + 0.015c \quad (38)$$

$$Amp_{HEA,Prediction} = 1 + 0.0088c + 0.0003c^2 \quad (39)$$

**Table 4**  
Amplification factor of elastic story drift formulas for each HEA profile as the story beam with RBS connections.

Profile type	Amplification factor of elastic drift formula
HEA100	$Amp = 1.00603 - 5.78942 \times 10^{-4}b - 5.36874 \times 10^{-3}c + 2.02188 \times 10^{-3}bc - 4.71652 \times 10^{-5}b^2 - 1.49952 \times 10^{-3}c^2$
HEA120	$Amp = 1.00668 - 5.59598 \times 10^{-4}b - 4.92893 \times 10^{-3}c + 1.59404 \times 10^{-3}bc - 3.92267 \times 10^{-5}b^2 - 1.23082 \times 10^{-3}c^2$
HEA140	$Amp = 1.00724 - 5.39093 \times 10^{-4}b - 4.61152 \times 10^{-3}c + 1.28818 \times 10^{-3}bc - 3.27379 \times 10^{-5}b^2 - 1.00143 \times 10^{-3}c^2$
HEA160	$Amp = 1.00782 - 4.48366 \times 10^{-4}b - 4.38970 \times 10^{-3}c + 1.08043 \times 10^{-3}bc - 2.85599 \times 10^{-5}b^2 - 8.44935 \times 10^{-4}c^2$
HEA180	$Amp = 1.00819 - 4.35334 \times 10^{-4}b - 4.11427 \times 10^{-3}c + 8.99608 \times 10^{-4}bc - 2.43626 \times 10^{-5}b^2 - 7.02413 \times 10^{-4}c^2$
HEA200	$Amp = 1.00863 - 3.62523 \times 10^{-4}b - 3.92950 \times 10^{-3}c + 7.78143 \times 10^{-4}bc - 2.18872 \times 10^{-5}b^2 - 6.10727 \times 10^{-4}c^2$
HEA220	$Amp = 1.00888 - 3.54333 \times 10^{-4}b - 3.72352 \times 10^{-3}c + 6.64300 \times 10^{-4}bc - 1.89910 \times 10^{-5}b^2 - 5.13836 \times 10^{-4}c^2$
HEA240	$Amp = 1.00914 - 3.00029 \times 10^{-4}b - 3.55837 \times 10^{-3}c + 5.77899 \times 10^{-4}bc - 1.69675 \times 10^{-5}b^2 - 4.41633 \times 10^{-4}c^2$
HEA260	$Amp = 1.00928 - 2.44616 \times 10^{-4}b - 3.37271 \times 10^{-3}c + 5.02217 \times 10^{-4}bc - 1.51662 \times 10^{-5}b^2 - 3.79384 \times 10^{-4}c^2$
HEA280	$Amp = 1.00941 - 2.31997 \times 10^{-4}b - 3.21500 \times 10^{-3}c + 4.44547 \times 10^{-4}bc - 1.37475 \times 10^{-5}b^2 - 3.34402 \times 10^{-4}c^2$
HEA300	$Amp = 1.00953 - 1.92780 \times 10^{-4}b - 3.07164 \times 10^{-3}c + 3.95106 \times 10^{-4}bc - 1.25743 \times 10^{-5}b^2 - 2.95008 \times 10^{-4}c^2$
HEA320	$Amp = 1.00908 - 1.43533 \times 10^{-4}b - 3.17887 \times 10^{-3}c + 3.55586 \times 10^{-4}bc - 1.05135 \times 10^{-5}b^2 - 2.03157 \times 10^{-4}c^2$
HEA340	$Amp = 1.00882 - 1.02015 \times 10^{-4}b - 3.31276 \times 10^{-3}c + 3.28031 \times 10^{-4}bc - 9.15688 \times 10^{-6}b^2 - 1.29342 \times 10^{-4}c^2$
HEA360	$Amp = 1.00863 - 6.82051 \times 10^{-5}b - 3.44612 \times 10^{-3}c + 3.06064 \times 10^{-4}bc - 8.15022 \times 10^{-6}b^2 - 6.59131 \times 10^{-5}c^2$
HEA400	$Amp = 1.00834 - 1.19286 \times 10^{-5}b - 3.69411 \times 10^{-3}c + 2.74056 \times 10^{-4}bc - 6.81002 \times 10^{-6}b^2 + 3.74028 \times 10^{-5}c^2$
HEA450	$Amp = 1.00795 + 3.52323 \times 10^{-5}b - 3.91277 \times 10^{-3}c + 2.40435 \times 10^{-4}bc - 5.62913 \times 10^{-6}b^2 + 1.40399 \times 10^{-4}c^2$
HEA500	$Amp = 1.00754 + 7.04571 \times 10^{-5}b - 4.07786 \times 10^{-3}c + 2.15408 \times 10^{-4}bc - 4.85605 \times 10^{-6}b^2 + 2.20687 \times 10^{-4}c^2$
HEA550	$Amp = 1.00707 + 1.04451 \times 10^{-4}b - 4.18573 \times 10^{-3}c + 1.97150 \times 10^{-4}bc - 4.35112 \times 10^{-6}b^2 + 2.83558 \times 10^{-4}c^2$
HEA600	$Amp = 1.01437 - 9.75063 \times 10^{-5}b - 5.08706 \times 10^{-3}c + 1.97558 \times 10^{-4}bc - 2.48135 \times 10^{-6}b^2 + 3.45208 \times 10^{-4}c^2$
HEA650	$Amp = 1.00591 + 1.58831 \times 10^{-4}b - 4.25330 \times 10^{-3}c + 1.68857 \times 10^{-4}bc - 3.66765 \times 10^{-6}b^2 + 3.77419 \times 10^{-4}c^2$
HEA700	$Amp = 1.00516 + 1.72092 \times 10^{-4}b - 4.19493 \times 10^{-3}c + 1.57912 \times 10^{-4}bc - 3.40000 \times 10^{-6}b^2 + 4.09822 \times 10^{-4}c^2$
HEA800	$Amp = 1.00364 + 2.37996 \times 10^{-4}b - 4.03271 \times 10^{-3}c + 1.38623 \times 10^{-4}bc - 3.10113 \times 10^{-6}b^2 + 4.63788 \times 10^{-4}c^2$
HEA900	$Amp = 1.00193 + 2.64777 \times 10^{-4}b - 3.75889 \times 10^{-3}c + 1.22140 \times 10^{-4}bc - 2.79244 \times 10^{-6}b^2 + 5.00731 \times 10^{-4}c^2$
HEA1000	$Amp = 1.00007 + 2.88034 \times 10^{-4}b - 3.38437 \times 10^{-3}c + 1.07808 \times 10^{-4}bc - 2.54393 \times 10^{-6}b^2 + 5.23493 \times 10^{-4}c^2$

$$Amp_{HEA,Design} = 1 + 0.011c \quad (40)$$

As displayed in Fig. 15, the maximum value of the amplification factor of elastic story drift between the beam profiles starts at about 0.8% and will eventually reach about 8%. Furthermore, from this figure it can be assured that an adequate safety margin is considered even in the worst-case scenario while using design Eqs. (38) and (40). Thus, these easy-to-use equations have the capability of utilizing by engineers or incorporating in steel structures design codes.

## 6. Expanding the application of the developed linear design formulas to plate girders

The primary purpose of this section is to evaluate the impact of web and flanges plates' thickness of built-up sections having some dimensional similarity to the rolled profiles used in this study (IPE and HEA profiles), on the amplification factor of elastic story drift. Then, according to the obtained results, a discussion toward extending the

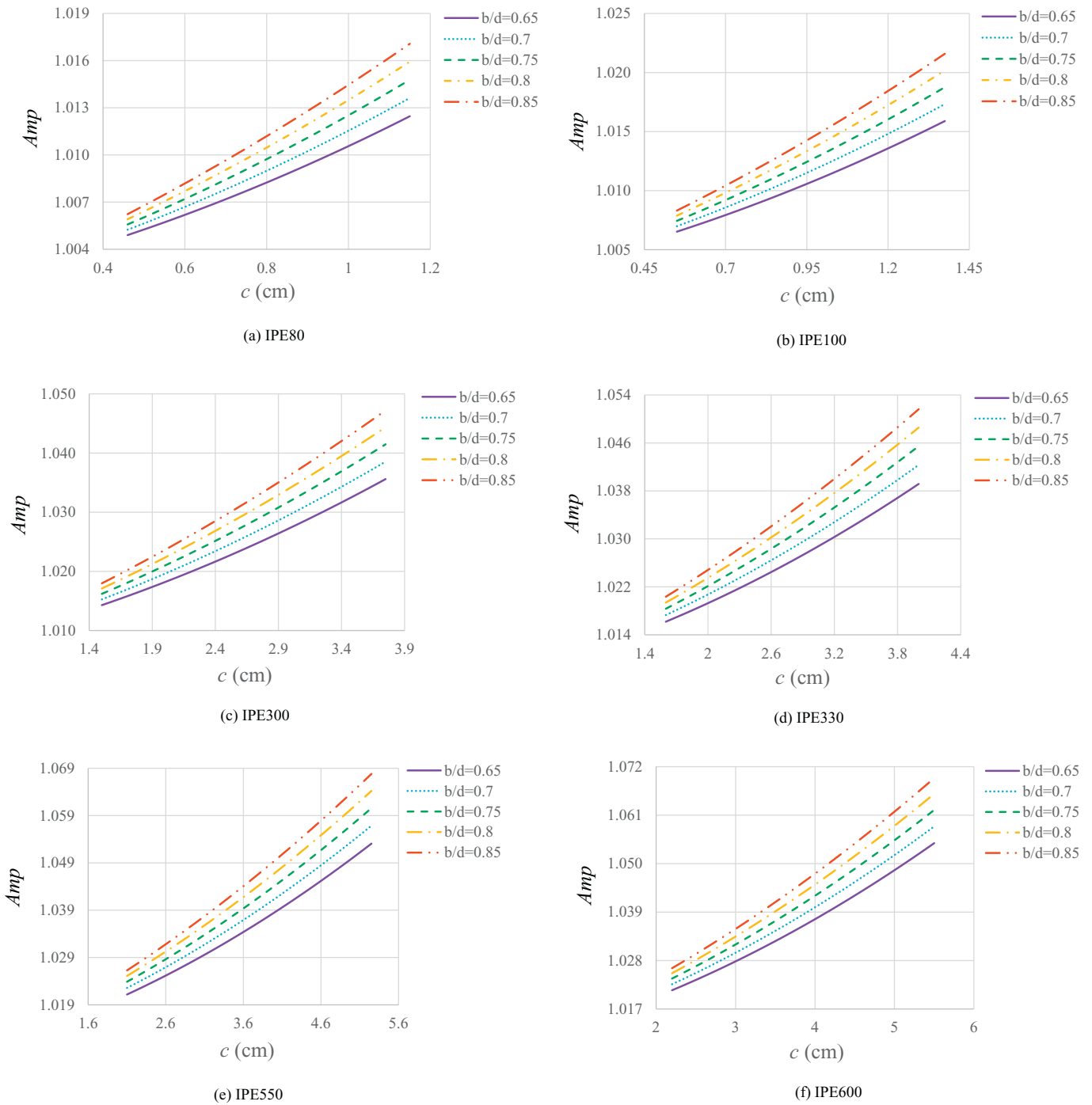


**Fig. 12.** Effect of the parameter *c* upon the amplification factor of elastic story drift when IPE profiles used as the story beam: (a) IPE80, (b) IPE100, (c) IPE300, (d) IPE330, (e) IPE550 and (f) IPE600.

application of the linear design formulas presented in the previous section to the desired built-up sections is conducted. Eventually, a method will be proposed for complete assurance of applicability of these equations to plate girders.

It is a generally held view that built-up sections are usually used in the building industry because of the unavailability of required rolled profiles or the limitations in the capacity and configuration of similar rolled profiles. In the following, four plate girder sections with RBS connections are analyzed using Eqs. (35), (38) and (40) to identify the influence of flanges and web plates' thickness on the amplification factor of elastic story drift. Two of these sections have the same height and flange width as IPE 300 and IPE 600 profiles, and the other two

have the same height and flange width as HEA 300 and HEA 1000 profiles, but with various flanges and web plates thicknesses.

AISC Seismic Provisions for Structural Steel Buildings [19] requires specific ranges of width to thickness ratio for web and flanges plates of the sections used in intermediate steel moment resisting frames (IMRFs) in which utilizing RBS connections are allowable. The maximum acceptable compactness ratios for flanges and web plates in an IMRF are defined by Eqs. (41) and (42), respectively.

$$\lambda_{md,f} = \frac{b_f}{2t_f} = 0.4 \sqrt{\frac{E}{R_y F_y}} \tag{41}$$

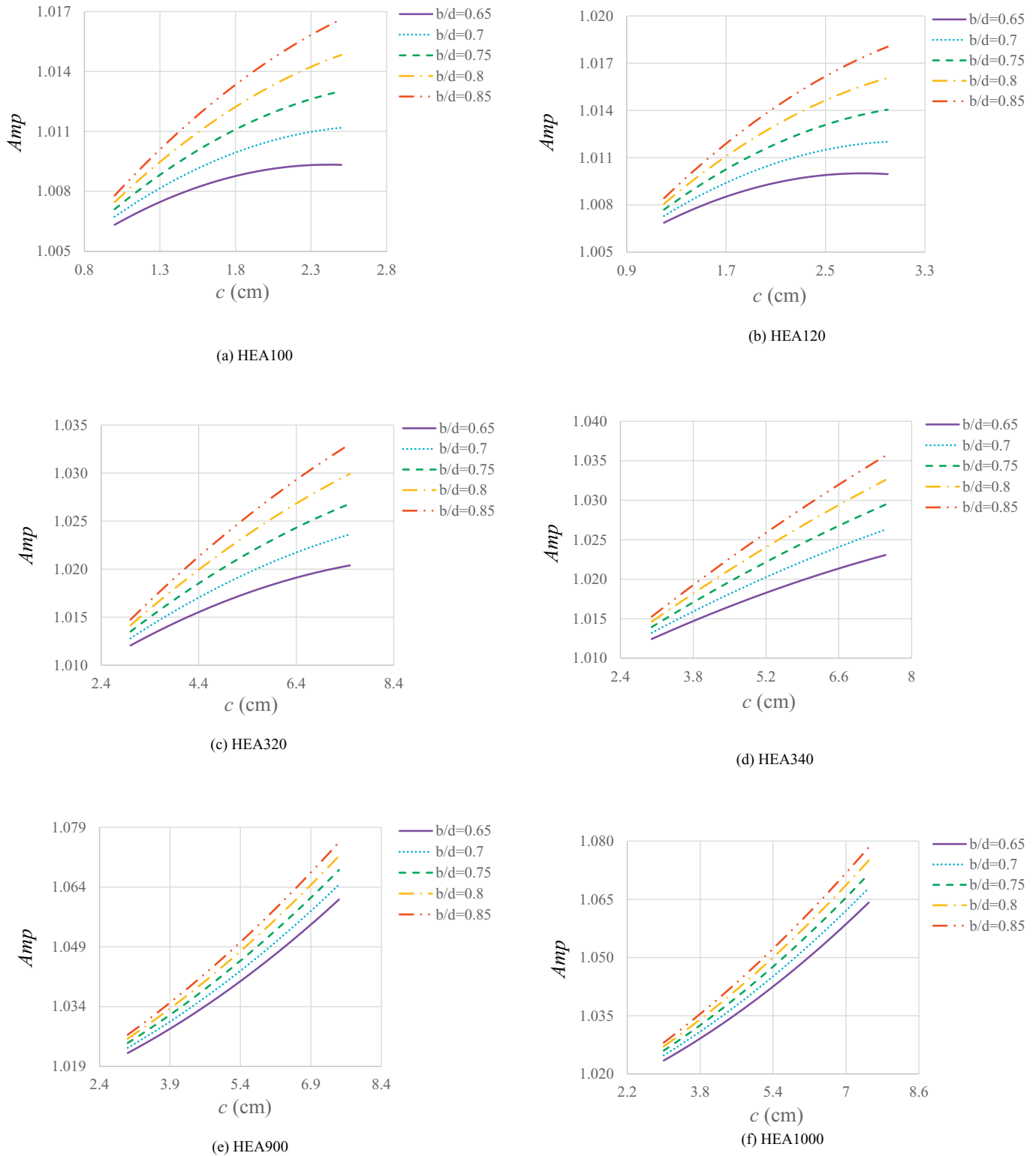


Fig. 13. Effect of the parameter *c* on the amplification factor of elastic story drift when HEA profiles used as the story beam: a) HEA100. b) HEA120. c) EA320. d) HEA340. (e) HEA900 and f) EA1000.

$$\lambda_{md,w} = \frac{h_w}{t_w} = 1.57 \sqrt{\frac{E}{R_y F_y}} \tag{42}$$

where,  $F_y$  and  $R_y$  are uniaxial yield stress and yield strength ratio of used steel, respectively. In the following parametric study, the steel grade

used in the built-up beam sections is considered ASTM A36. Moreover, one of the thicknesses of flange and web plates is kept constant having minimum usable values which satisfy Eqs. (41) and (42), respectively; meanwhile, 3 different values are assumed for the other thickness based on these equations. The geometric parameters of these sections, as well as the amplification factors of elastic story drift resulting from Eqs. (35), (38) and (40) are illustrated in Table 5.

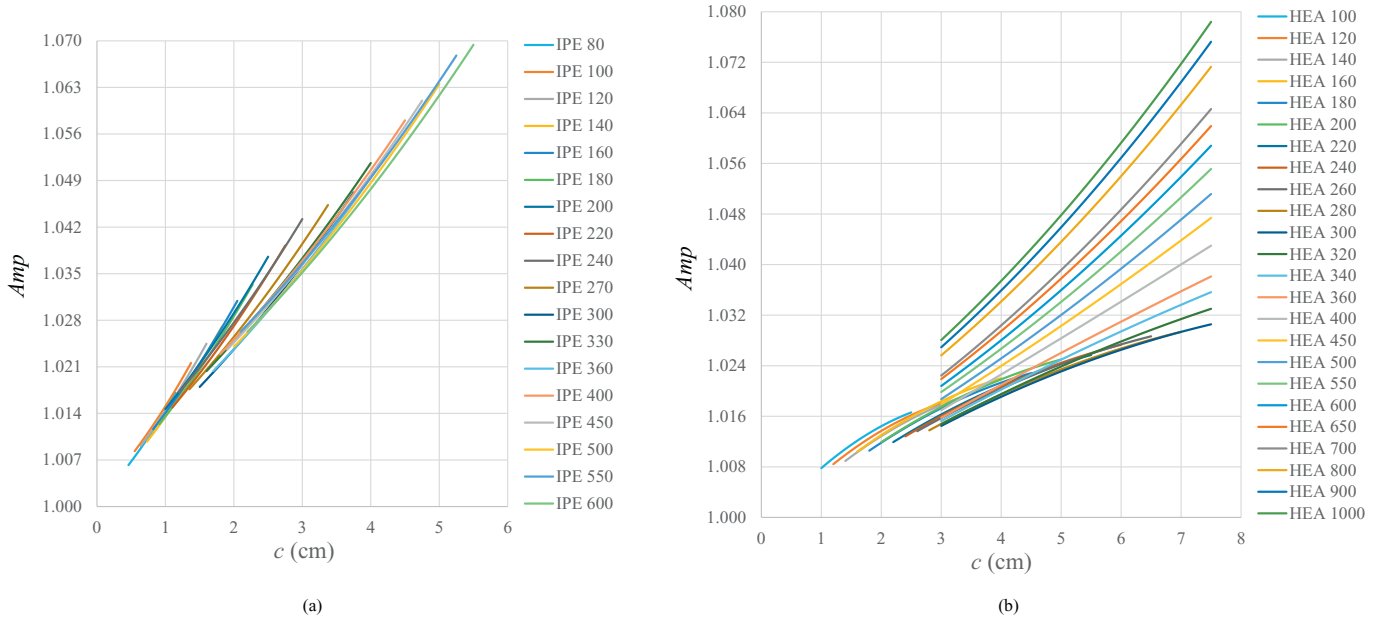


Fig. 14. Putting together all curves of the amplification factor of elastic story drift whose  $b/d = 0.85$ : a) IPE profiles curves whose  $b/d = 0.85$  and b) HEA profiles curves whose  $b/d = 0.85$ .

As can be seen in Table 5, the maximum variations in the maximum amplification factor of elastic story drift are between 0.9% and 1.6% among the plate girders. Given utilizing the IPE and HEA profiles with specific flanges and web plates' thickness to develop the linear design formulas along with the conservative and reasonable safety margin provided in this process, it is evident that the effects of web and flanges

plates' thickness in built-sections dimensionally similar to the IPE and HEA profiles, can be neutralized by these formulas.

At a rough estimate, due to the conspicuous effect of parameter  $c$  ( $0.1b_f \leq c \leq 0.25b_f$ ) in comparison with the parameter  $b$  ( $0.65d \leq b \leq 0.85d$ ), and capability of the linear design formulas so as to neutralize the impact of the beam web and flanges plates' thickness on the amplification factor of elastic story drift, it can be stated that if the flange width of a built-up beam is in the flange width range of IPE profiles ( $b_{f IPE80} = 4.6 \text{ cm} \leq b_f \leq b_{f IPE600} = 22 \text{ cm}$ ) or HEA profiles ( $b_{f HEA100} = 10 \text{ cm} \leq b_f \leq b_{f HEA1000} = 30 \text{ cm}$ ), Eqs. (38) and (40) may offer a correct response to the built-up beam, respectively. However, in the following, a fully guaranteed method is suggested for applying these equations to plate girders.

With respect to the effects of the parameters  $c$  and  $b$  on the amplified elastic story drift, flange width and total height of a beam with RBS

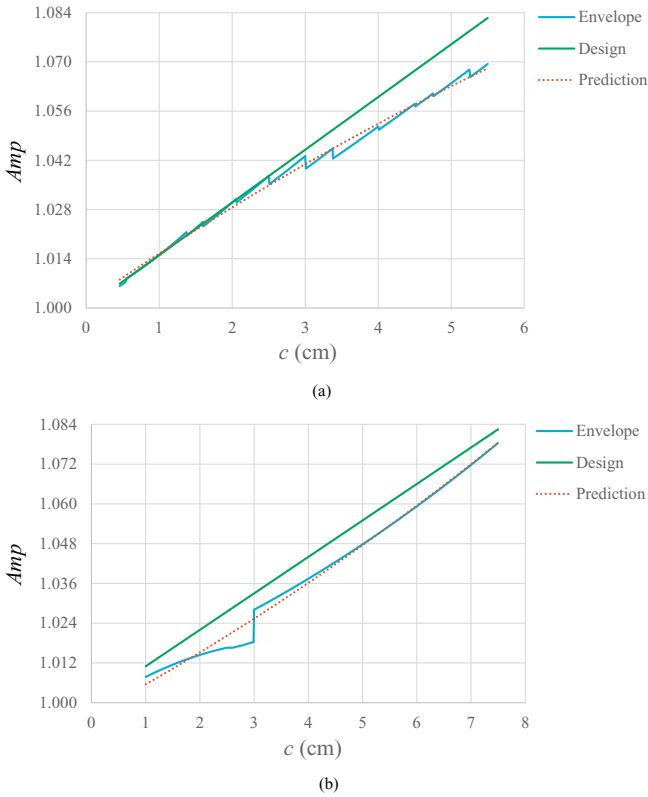


Fig. 15. Diagrams of the amplification factor of elastic story drift formulas for design and prediction purposes when: a) IPE profiles are used as the story beam and b) HEA profiles are used as the story beam.

Table 5  
Geometrical characteristics of the built-up sections and their influence on the maximum amplification factor of elastic story drift.

Built-up sections' geometrical parameters				Maximum amplification factor of elastic story drift	
$d$ (cm)	$b_f$ (cm)	$t_f$ (cm)	$t_w$ (cm)	$Amp$	$Amp_{Design}$
30	15	0.8	0.8	1.039	
30	15	1.5	0.8	1.042	
30	15	2.5	0.8	1.040	$Amp_{IPE \text{ design}} = 1.056$
30	15	0.8	1.2	1.036	
30	15	0.8	1.5	1.033	
30	30	2	0.8	1.024	
30	30	3	0.8	1.021	
30	30	4	0.8	1.019	$Amp_{HEA \text{ design}} = 1.0825$
30	30	2	1.2	1.028	
30	30	2	1.5	1.030	
60	22	1.2	1.5	1.055	
60	22	1.5	1.5	1.058	
60	22	2.5	1.5	1.062	$Amp_{IPE \text{ design}} = 1.0825$
60	22	1.2	2	1.050	
60	22	1.2	2.5	1.046	
100	30	2	2.5	1.066	
100	30	3	2.5	1.073	
100	30	4	2.5	1.075	$Amp_{HEA \text{ design}} = 1.0825$
100	30	2	3	1.062	
100	30	2	3.5	1.059	

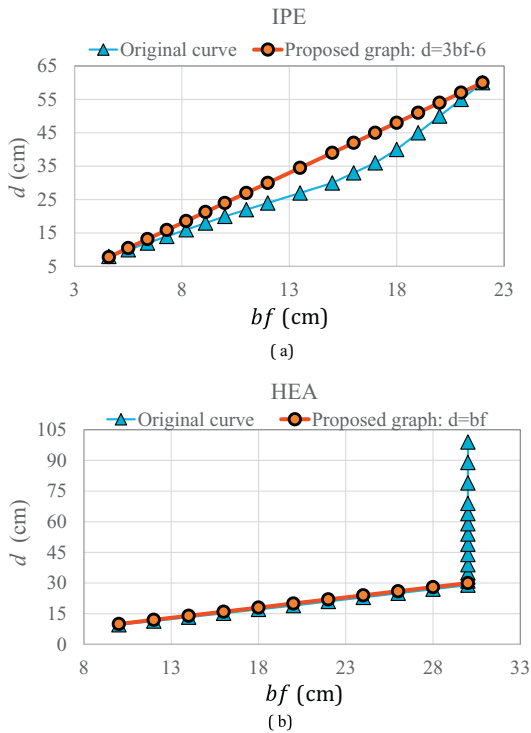


Fig. 16. Relationship between flange width and section height when: (a) IPE profiles are used as the story beam and (b) HEA profiles are used as the story beam.

$$\text{If } 4.6 \text{ cm} \leq b_f \leq 22 \text{ cm} \rightarrow d \leq 3b_f - 6 \quad (43)$$

$$\begin{cases} \text{If } 10 \leq b_f < 30 \rightarrow d \leq b_f \\ \text{If } b_f = 30 \rightarrow d \leq 100 \end{cases} \quad (44)$$

connections used in each story of a steel moment frame, are two geometrical parameters with the great effects on the maximum amplification factor of elastic story drift correspondingly. By examining the relationship between IPE and HEA profiles' flange width and total height, regarding that the linear design formulas are able to neutralize the effects of web and flange plates' thickness, the application of these formulas can also be extended to plate girders. Fig. 16 depicts the relationship between the flange width and section total height in HEA and IPE profiles. According to the diagrams, if the considered plate girder can fulfill the conditions presented in Eqs. (43) and (44) it can be surely stated that using the Eqs. (38) and (40) respectively, yields the right answers for this plate girder with an acceptable margin of safety. But, if the mentioned conditions are not satisfied, the parameter  $c$  or  $b$  value may exceed the ranges investigated in this research and Eqs. (38) and (40) may not respond properly.

## 7. Conclusions

In this study, a precise and improved approach using mathematical procedures along with structural analysis rules is adopted to determine the amount of amplified elastic drift or the percentage of stiffness variations in a typical story of steel moment frames with RBS connections as well as proposing practical formulas in this field. Following verification of the accuracy of proposed method for calculating the variable moment of inertia along the RBS connection region by numerical modeling, numerous sensitivity analyses have been conducted to determine the most effective RBS connection parameters on the elastic drift of steel moment frames, and then by using a statistical approach known as response surface method accompanied by premises considered in a previous authentic research and the developed method, two linear formulas are derived for computing the amplification factor of elastic story drift

based on the use of IPE or HEA beam with RBS connections in the intended story. In the last section, the application of these formulas has become more general and expanded to built-up beam sections as well. The most important results of this research are as follows:

1. In this paper, an improved analytical method and simple linear formulas are proposed for determining the actual value of amplified elastic drift and the amplification factor of elastic drift in a story of steel moment frames with RBS connections, respectively. According to the obtained results, the percentage of stiffness reduction or amplification of elastic drift induced by RBS connections in a story of steel moment frames is negligible, however, a proper evaluation of the exact amount of these factors helps to come up with an optimum design of the structure and better identification of RBS connections' elastic behavior.
2. The sensitivity analyses to determine effects of the RBS connection parameters on the elastic drift regarding the use of IPE or HEA profiles as the beam, showed that the parameter  $a$  has a very small effect on the elastic drift response. The parameters  $b$  and  $c$  have been recognized as the most influential parameters in the elastic drift of steel moment frames, but their effects are not the same. Generally, the parameter  $c$  has a greater effect than the parameter  $b$  on the elastic inter-story drift. Note that by increasing the height of the beam profile relative to its flange width, the effect of the parameter  $c$  on the elastic inter-story drift gradually increases compared with the effect of the parameter  $b$ .
3. The quadratic formulas obtained via the RSM method to compute the amplification factor of elastic drift in a story with each of IPE and HEA beams and RBS connections, have the lack of fit and pure error approximately equal to zero and curve fitting about 99%. This denotes the high accuracy and reliability of these formulas derived from the suggested method in this research. Moreover, the linear design formulas proposed in this study are easy-to-use and have adequate conservative consideration with regard to uncertainties. This issue is concluded from the linear design formulas diagrams which have positions upper than the envelopes of the curves whose  $b/d = 0.85$ . The results of this research also illustrated that the values of the amplification factor of elastic drift in a story having IPE or HEA beams with RBS connections, are approximately from 0.8% to 8%. All in all, regarding the simplicity of the use, accuracy and conservative estimation of the linear design formulas, they can be utilized by designers and codes.
4. Proposed linear formulas are capable of calculating the amplification factor of elastic drift or the percentage of stiffness reduction in a typical story of steel moment frames with RBS connections in the case of using IPE or HEA beams in the story, but these formulas can also be utilized when having a story beam (rolled or plate) with the similar size and shape as the profiles used in this research.
5. The method of calculating the variable moment of inertia along the RBS connection region presented in this research is capable of adopting in future studies in order to compute flexural rigidity variations whenever RBS connections are used as part of a system such as double RBS connections or combination of RBS connections with the steel plate shear wall in a dual system.
6. According to the parametric analyses carried out in this study on the plate girders dimensionally similar to HEA and IPE profiles (i.e. in height and flange width) and having RBS connections, the maximum effect of flanges and web plates' thickness on the maximum amplification factor of elastic story drift was between 0.9% and 1.6% among these profiles.
7. Application of the linear design formulas proposed for calculating the amplification factor of elastic story drift while using HEA and IPE profiles as the story beam, can even be expanded to the plate girders. Considering the appropriate safety margin of these formulas, they are capable of entailing the effects induced by changes in the thickness of flanges and web plates provided that the plate

girder's height and flange width would be similar to IPE and HEA profiles. At a rough estimation, these formulas may result in the correct response for a plate girder when the flange width of this profile is in the flange width range of IPE or HEA profiles. But meeting the requirements demonstrated in Eqs. (43) and (44) assures the validity of applying Eqs. (38) and (40), respectively; to plate girders.

## References

- [1] American Institute of Steel Construction (AISC), *Seismic Provisions for Structural Steel Buildings*, Chicago) 1997.
- [2] A. Plumier, The dogbone: back to the future, *Eng. J. Am. Inst. Steel Constr.* 34 (1997) 61–67.
- [3] N.R. Iwankiw, C.J. Carter, The dogbone: a new idea to chew on, *Mod. Steel Constr.* 36 (1996) 18–23.
- [4] S.J. Chen, C.H. Yeh, J.M. Chu, Ductile steel beam-to-column connections for seismic resistance, *J. Struct. Eng.* 122 (1996) 1292–1299.
- [5] M.D. Engelhardt, T. Winneberger, A.J. Zekany, T.J. Potyraj, Experimental investigation of dogbone moment connections, *Engl. J.* 35 (1998) 128–139.
- [6] E.P. Popov, T.S. Yang, S.P. Chang, Design of steel MRF connections before and after 1994 Northridge earthquake, *Eng. Struct.* 20 (1998) 1030–1038.
- [7] R. Montuori, The influence of gravity loads on the seismic design of RBS connections, *Open Constr. Build. Technol. J.* 8 (2014) 248–261.
- [8] P. Castaldo, B. Palazzo, F. Perri, FEM simulations of a new hysteretic damper: the dissipative column, *Ing. Sismica.* 33 (2015) 34–45.
- [9] D.T. Pachoumis, E.G. Galoussis, C.N. Kalfas, A.D. Christitsas, Reduced beam section moment connections subjected to cyclic loading: experimental analysis and FEM simulation, *Eng. Struct.* 31 (2009) 216–223.
- [10] J.J. Chambers, S. Almudhafar, F. Stenger, Effect of reduced beam section frame elements on stiffness of moment frames, *J. Struct. Eng.* 129 (2003) 383–393.
- [11] F. Thompson, G.G. Haywood, *Structural Analysis Using Virtual Work*, vol. 202, Taylor & Francis, 1986.
- [12] C.K. Wang, *Intermediate Structural Analysis*, McGraw-Hill Inc, Singapore, 1983.
- [13] C.H. Lee, S.W. Chung, A simplified analytical story drift evaluation of steel moment frames with radius-cut reduced beam section, *J. Constr. Steel Res.* 63 (2007) 564–570.
- [14] AISC, *Prequalified Connections for Special and Intermediate Steel Moment Frames for Seismic Applications*, AISC/ANSI 358–16, American Institute of Steel Construction (AISC), Chicago, IL, 2016.
- [15] Maple 18, Maplesoft, A Division of Waterloo Maple Inc, 2014.
- [16] MathWorks, Inc, *MATLAB and Statistics Toolbox Release*, The MathWorks, Natick, MA, 2012.
- [17] Abaqus, Ver. 6.14 Documentation, Dassault Systemes Simulia Corporation, 2014 651.
- [18] AISC, *Specification for Structural Steel Buildings*, AISC/ANSI 360–16, American Institute of Steel Construction (AISC), Chicago, IL, 2016.
- [19] AISC, *Seismic Provisions for Structural Steel Buildings*, AISC/ANSI 341–16, American Institute of Steel Construction (AISC), Chicago, IL, 2016.
- [20] de Normalisation CE, *Eurocode 3–Design of Steel Structures–Part 1. 5: General Rules and Supplementary Rules for Plated Structures*, 2006 (EN1993-1-5, Brussels; ).
- [21] H. Krawinkler, Shear in beam-column joints in seismic design of steel frames, *Engl. J.* 15 (1978).
- [22] Design-Expert® software, Version 7, Stat-Ease, Inc, Minneapolis, MN, USA, 2005.